ETH

Eidgenössische Technische Hochschule Zürich
Swiss Federal Institute of Technology Zurich

Declaration of originality

The signed declaration of originality is a component of every semester paper, Bachelor's thesis, Master's thesis and any other degree paper undertaken during the course of studies, including the respective electronic versions.

Lecturers may also require a declaration of originality for other written papers compiled for their courses.

I hereby confirm that I am the sole author of the written work here enclosed and that I have compiled it in my own words. Parts excepted are corrections of form and content by the supervisor.

Title of work (in block letters):

CONTROL OF DISTRIBUTED ELECTRIC WATER HEATERS FOR ANCILLARY SERVICES PROVISION IN THE POWER GRID

Authored by (in block letters):

For papers written by groups the names of all authors are required.

Name(s):	**First name(s):**
MARTINEZ GOMEZ	ADRIAN

With my signature I confirm that

- I have committed none of the forms of plagiarism described in the 'Citation etiquette' information sheet.
- I have documented all methods, data and processes truthfully.
- I have not manipulated any data.
- I have mentioned all persons who were significant facilitators of the work.

I am aware that the work may be screened electronically for plagiarism.

Place, date	**Signature(s)**
Zurich, 17/04/2015	

For papers written by groups the names of all authors are required. Their signatures collectively guarantee the entire content of the written paper.

Master Thesis

Control of distributed electric water heaters for ancillary services provision in the power grid

Automatic Control Laboratory
Swiss Federal Institute of Technology (ETH) Zurich

Adrian Martinez Gomez

Supervision

Maryam Kamgarpour
Evangelos Vrettos

Professor

Prof. John Lygeros

March 2015

Contents

Abstract

The increasing penetration of renewable energy resources into the power grid has posed a variety of new challenges for their smart employment. Thermostatically controlled loads are of high interest due to their ability to store energy in the form of heat. Aggregated populations of such devices have been introduced as part of demand side management control strategies, to steer the power of these electrical devices. The ability of such an aggregated system to balance the behaviour of intermittent renewable resources is of high interest. In this project, modeling and control design of such an aggregated system is addressed. The type of devices studied is the electric water heater. System identification techniques are developed to achieve a population model, measuring the aggregate power consumption after application of a previously defined external control signal. Finally, a controller is implemented to steer the power output of the population to track a desired reference trajectory. This controller performs well with reference signals of reasonable duration. Also, to ensure good performance sufficient recovery time for the system dynamics due to previous controller disturbances has to be maintained.

Nomenclature

Symbols

α	Affine cost term	
β	Linearity coefficient	
$\mathbf{m}_{\text{cat}}$	Water mass categories	[kg]
$\mathbf{P}_{\text{cat}}^{\text{rated}}$	Rated power per category	[kW]
$\mathbf{p}_{\text{cat}}$	Category shares	[%]
δ	Temperature deadband	[K]
$\dot{m}_{\text{day}}$	Hot water flow rate	$[\frac{\text{kg}}{\text{s}}]$
ϵ	Prediction error for the ARMAX model	
η	Electrical efficiency coefficient	[%, -]
γ	Input-output mapping function	
$\hat{u}$	External control signal	[-]
$\hat{y}$	Predictor for the output $\tilde{y}$	
$[lb, ub]$	Lower and upper bound for the optimization constraints	
$\left[\mathbf{m}_{\text{daily,cat}}^{\text{min}}, \mathbf{m}_{\text{daily,cat}}^{\text{max}}\right]$	Daily draw bounds per category	[kg]
$\left[\delta^{\text{min}}, \delta^{\text{max}}\right]$	Deadband size bounds	[K]
$[A_{\text{eq}}, b_{\text{eq}}]$	Equality constraint matrix and vector	

$[A_{\text{ineq}}, b_{\text{ineq}}]$ Inequality constraint matrix and vector

$\left[T_{\text{set}}^{\min}, T_{\text{set}}^{\max}\right]$ Temperature set-point bounds [°C]

$\left[U^{\min}, U^{\max}\right]$ Heat loss coefficient bounds $[\frac{W}{m^2 K}]$

$\{n, m, \bar{m}, q\}$ ARMAX model orders

$\mathbf{A}_k$	System state matrix for an individual EWH	
$\mathbf{B}_k$	System control matrix for an individual EWH	
$\mathbf{T}_0$	Initial temperature vector	[°C]
$\mathbf{t}_{\text{draw}}$	Vector of time instants when a draw takes place	[s]
$\mathbf{T}_k$	Temperature vector for an individual EWH	[°C]
$\mathcal{M}_{h_{\text{start}}}$	ARMAX model for starting hour h_{start}	
$\mathcal{P}$	EWH population	
$\mathcal{S}_{h_{\text{start}}}$	State-space model for starting hour h_{start}	
$\mathcal{U}$	Space for the input signals	
$\mathcal{W}$	Space of the exogenous input averaged water draws	
$\mathcal{X}$	State space	
$\mathcal{Y}$	Space for the output signals	
$\mu_{N_{\text{app}}}$	Mean of the aggregate power for N_{app} EWHs	
$\overline{\mathcal{M}}$	Set of all time dependant ARMAX models	
Φ	Grouped values for the regressor φ	
ρ	Density	$[\frac{\text{kg}}{\text{m}^3}]$
ρ_{ref}	Minimum between the average density of the water layers above i and density ρ^{i+1}	$[\frac{\text{kg}}{\text{m}^3}]$
σ_{noise}	Standard deviation for the noise signal e	
$\sigma_{N_{\text{app}}}$	Standard deviation of the aggregate power for N_{app} EWHs	
θ	Parameter vector	

$\tilde{\mathcal{Y}}$	Space for the normalized output signals	
$\tilde{P}_{\text{agg}}$	Normalized aggregate power	[-]
$\tilde{y}$	Normalized output signal	[-]
$\triangle \mathbf{t}_{\text{draw}}$	Vector of intervals between water draw events	[$\triangle$s]
$\triangle \mathbf{t}_{\text{duration}}$	Vector of intervals draw duration times	[$\triangle$s]
$\triangle t$	Mesh in time	[s]
$\triangle x$	Mesh in space	[m]
ε_{eff}	Internal heat generation	[-]
φ	Regressor vector	
$\widetilde{k}$	Heat loss coefficient	$[\frac{1}{\text{s}}]$
$\widetilde{k}'$	Heat loss coefficient of top and bottom layers	$[\frac{1}{\text{s}}]$
ξ	Uniformly distributed random number for probability switching	
a	Water thermal diffusivity	$[\frac{\text{m}^2}{\text{s}}]$
$A\left(z\right)$	Auto-regressive (AR) polynomial for ARMAX model	
b	Friction parameter	$[\frac{\text{kg}}{\text{s}}]$
$B_1\left(z\right)$	External input $\hat{u}$ polynomial for ARMAX model	
$B_2\left(z\right)$	Exogenous input polynomial for w^{ave} for ARMAX model	
c	Specific heat capacity of water	$[\frac{\text{J}}{\text{kg}\cdot\text{K}}]$
$C\left(z\right)$	Moving-Average (MA) polynomial for ARMAX model	
e	Noise signal for the ARMAX model	
F^b	Buoyant force	[N]
F^v	Viscous force	[N]
G	Plant of the system	
g	Gravitational constant	$[\frac{\text{m}^2}{\text{s}}]$

h_{start}	Starting time of an interval	[hour]
$J_{0\to N}$	Cost function	
m^i	Water mass of layer i	[kg]
m_{day}	Daily water usage	[liters]
N_{app}	Number of TCLs in the population	
n_{daily}	Total number of water draws per day	
$n^{\text{ave}}_{\text{hourly}}$	Hourly averaged draw probability	
N_{OFF}	Set of EWHs in a population that are OFF	
N_{ON}	Set of EWHs in a population that are ON	
N_{sim}	Number of simulation steps	
N_E	Number of experiments	
p	Terminal cost	
P^{ref}	Reference signal for optimization	
P_{agg}	Aggregate power	[kW]
p_{draw}	Probability of a draw event	[%]
Q	Quadratic cost term	
q	Stage cost	
$Q\left(.,.\right)$	Internal heat generation	$[\frac{\text{m}^2}{\text{s}}]$
R	Linear cost term	
r	Mixing ratio	[-]
T	Temperature	[°C]
T_{a}	Ambient temperature	[°C]
T_{cw}	Temperature at the water inlet	[°C]
T_{draw}	Water draw duration	[s]

$T_{\max}$	Upper temperature thresholds of the temperature deadband	[°C]
$T_{\min}$	Lower temperature thresholds of the temperature deadband	[°C]
T_{sample}	Sampling time	[s]
T_{set}	Set-point temperature	[°C]
$T_{n_{\text{heat}}}$	Temperature of heating element layer	[°C]
U^i	Velocity from the previous time step for layer i	$[\frac{\text{m}}{\text{s}}]$
$U_{0\to N}$	Input trajectory	
u_k	Internal switch controller	[-]
V	Vertical water velocity during water draws	$[\frac{\text{m}^2}{\text{s}}]$
w_i	Random water draw of experiment i	$[\frac{\text{liters}}{\text{min}}]$
Y	Grouped values for the output signal $\tilde{y}$	
y	Output signal	[kW]
y_{ARMAX}	Output generated by the ARMAX model	[-]
$y^{\text{ave}}_{\text{baseline}}$	Averaged baseline for aggregate power consumption in the autonomous case	[kW]
y_{measured}	Aggregate power measured for the population in open-loop, with external control	[kW]
z	Optimization variable	
I	Time interval	[hour]

Indices

ϑ	EWH index for the population
i	Layer index within the EWH model; Experiment index
k	Discrete time
n	Number of layers within the water heater

n_{heat}	Layer with heating device
$n_{\text{thermostat}}$	Layer with thermostat
t	Continuous time
long	For long water draws
medium	For medium water draws
short	For short water draws

Acronyms and Abbreviations

$\mathcal{N}$	Normal distribution with mean μ and variance σ^2
AC	Air Conditioner
ARMAX	Auto-Regressive-Moving-Average with eXogenous inputs model
DSM	Demand Side Management
DSM	Load Management
EWH	Electric Water Heater
Exp	Exponential distribution with parameter λ
HVAC	Heating, Ventilating, Air Conditioning unit
MAPE	Mean Average Percentage Error
MPC	Model Predictive Controller
MVC	Minimum Variance Controller
NRMSE	Normalized Root Mean Squared Error
ODE	Ordinary Differential Equation
PDE	Partial Differential Equation
RMSE	Root Mean Squared Error
SCQP	Sequential Convex Quadratic Program
TCL	Thermostatically Controlled Load
Unif	Uniform distribution

Chapter 1

Introduction

Aggregated populations of Thermostatically Controlled Loads (TCLs) (for example in the form of Air Conditioners (ACs), fridges, or Electric Water Heaters (EWHs)) have been introduced as part of Demand Side Management (DSM) strategies to control the power of electrical devices.
TCLs are very suitable for Load Management (LM), as they also add a degree of flexibility to DSM. This is due to their ability to store energy in the form of heat (in a sense, they work similarly to a battery). TCLs can *increase* power consumption with this storing feature.
For EWHs, the load type studied in this thesis, local controllers maintain the tank temperature within a deadband, using an internal ON/OFF switch control.

To develop an aggregate population model for the TCLs, while maintaining a good trade-off between accuracy and computational performance for the controller, is hard. Moreover, these aggregate models result from precisely modeling individual TCLs.
There is a variety of proposed simplified TCL models based on Ordinary Differential Equations (ODEs), as for example [1, 2, 3, 4]. On a step further, the two-layer EWH model studied by Kondoh et al. [5] is interesting, as it adds detailed modeling. However, it fails to model the internal water temperature dynamics in detail, as well as convection and conduction inside the water tank. Vrettos et al. [6] proposed a detailed model, by partitioning the inside of the water tank into n different temperature layers . This model is the one selected and studied throughout this project in Chapters 2 and 3, due to its high level of detail.

A challenge for EWHs compared to other TCLs are the stochastic water draws. Every time a consumer places a hot water draw, the dynamics within the tank change and cool water has to be added. Section 2.4 shows an approach to modeling these.

Once the individual load model is selected, the next step is to derive a *simplified* aggregate population model.
Some possible approaches to model the aggregate population are:

- To discretize the temperature deadband and use a Markov-chain model. This discretization is widely used, as for example in the projects [2, 7, 8, 4]. A more advanced approach on this is done by Kizikale et al. [9]
- In the work done by Callaway [10], aggregate TCL power consumption is manipulated by thermostat set-point control, and a statistical model is used to gain knowledge about the system dynamics. This ARMAX model is investigated in detail, and a minimum variance controller is derived.
- Use a simplified model developed from first principles, as done by Perfumo et al. [1]. In that instance, the model was developed for a homogenous population of ACs.

The ability to precisely control such a population for aggregate power tracking, to follow a desired power trajectory, is of extreme interest to the grid operator. The next step, once a model is selected, is to define an appropriate controller. A typical implementation of the controller is the Model Predictive Controller (MPC). Totu et al. [11] developed an algorithm based on this controller structure, as well as Koch et al. [8].
Its main advantages are the handling of system constraints and its high performance. As challenges, the implementation of such an MPC controller in real-time is dependant of the sampling interval of the system; the closed-loop stability is not automatically guaranteed. Also, the optimization problem could become infeasible.

The rest of this thesis is organized as follows: Chapter 2 deals with the modeling of one load, using Vrettos et al.'s [6] approach. Chapter 3 develops a population model, introducing the characterization of the baseline consumption and the concept of the external control signal. Next, Chapter 4 uses System Identification techniques to develop a characterization of the aggregate system so that in

Chapter 5 an efficient MPC-based controller can be implemented.
Figure 1.1 presents an overview of the organization of this thesis.

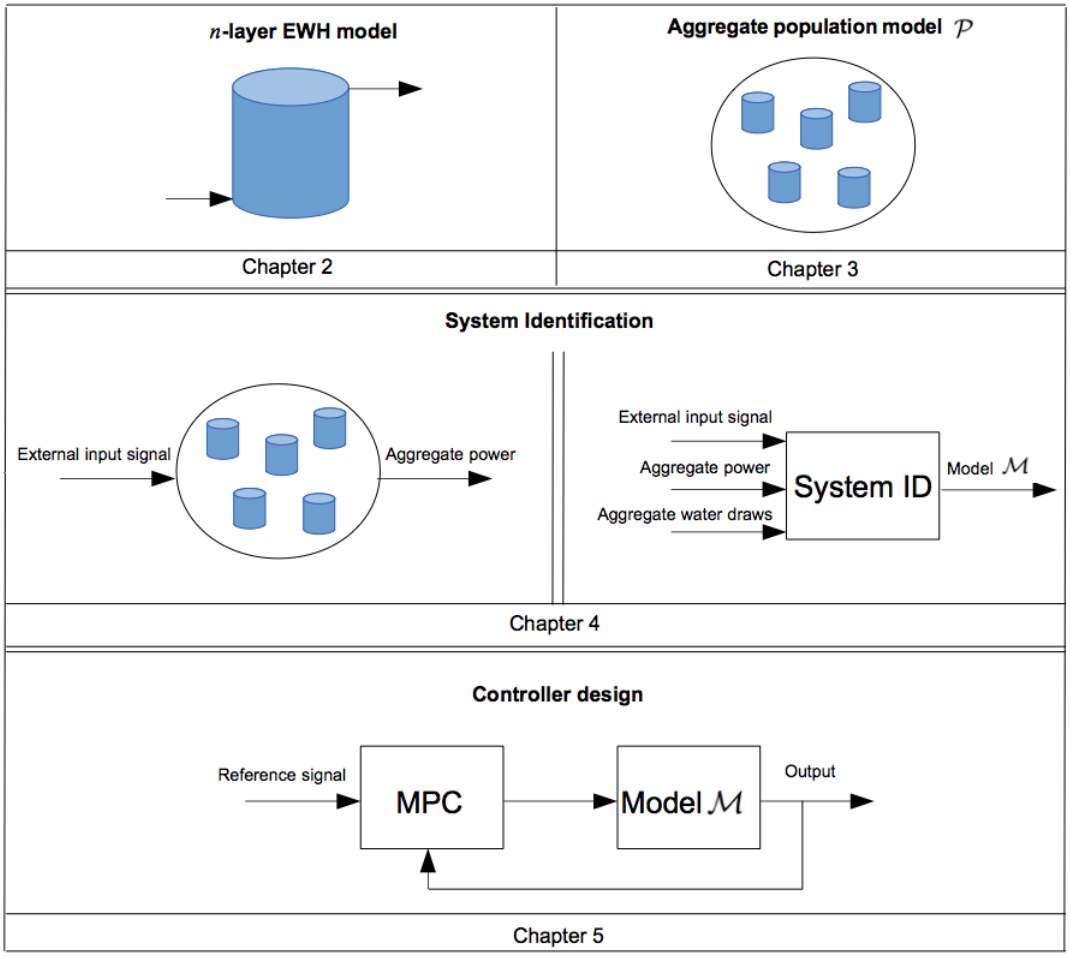

Figure 1.1: Overview of this thesis

Lastly, Table 1.1 shows an overview of the existing literature and their modeling and control approaches, to depict an overview of the current research state of this area.

Paper	**Device type**	**Load dynamics**	**Noise**	**Population**	**Controller**
[10]	Wind turbines	Hybrid ODE	$\surd$	Heterogeneous	MVC
[1]	HVACS (focus AC)	Hybrid ODE	$\surd$	Homogeneous	Cluster-based controller
[4]	ACs (cooling)	ODE model	X	Both	Locked states
[12]	HVACs	Discrete time difference eq.	$\surd$	Heterogeneous	Control gain with forecasting
[2]	ACs (cooling)	Hybrid ODE	X	Homogeneous	Lyapunov output tracking
[5]	EWHs	ODE; 2-layer model	$\surd$	Homogeneous	Custom switching controller
[6]	EWHs	PDE; n-layer model	$\surd$	Heterogeneous	4 different controllers
[8]	HVACs (cooling and heating)	Discrete time difference eq.	$\surd$	Heterogeneous	MPC
[13]	HVACs (cooling)	Stochastic hybrid unit model	$\surd$	Both	*Open-loop*
[3]	Buildings	ODE model	X	Homogeneous	*Not addressed*
[7]	Cooling loads	Hybrid ODE	X	Homogeneous	LQR
[**?**]	EWHs	6-layer model	X	*None*	*Not addressed*
[9]	EWHs	Stochastic dynamic agents	$\surd$	Heterogeneous	Local controllers (Nash eq.)

Table 1.1: Probabilistic parameters for the water draws

Chapter 2

Individual Electric Water Heater model

In this Chapter, the dynamical model for an individual Electric Water Heater (EWH) is presented. This model described the thermal stratification present inside the water tank and was developed by Vrettos et al. [6] and Koch [14]. This model's key feature is the partition of the tank into n different heat layers, which provides greater modeling detail. The model also takes into account the internal heat generation and the turbulent mixing at the tank inlet. These are detailed assets compared to other models developed in the literature. For example, Kondoh et al. [5] assumed a simplified two-layer model, with a thin mixing layer artificially placed between these two layers.
Therefore, it is reasonable to use the model developed by Vrettos et al. throughout this project as an accurate approximation of an EWH.

2.1 Laminar flow scheme

The one dimensional Partial Differential Equation (PDE) determining the laminar temperature flow in the water storage tank is given by Dinçer et al. [15]:

$$\frac{\partial T}{\partial t} + V\frac{\partial T}{\partial x} = a\varepsilon_{\text{eff}}\frac{\partial^2 T}{\partial x^2} - \tilde{k}\left(T - T_{\text{a}}\right) + Q\left(x,t\right), \tag{2.1}$$

where x stands for the position along the vertical axis of the tank, T is the temperature, t denotes time, V is the vertical water velocity during water draws, a

is the thermal diffusivity, $\tilde{k}$ is the heat loss coefficient, T_{a} accounts for the ambient temperature, $Q\,(x,t)$ corresponds to the internal heat generation, and $\varepsilon_{\mathrm{eff}}$ denotes the turbulent mixing at the tank inlet, which can be laminar ($\varepsilon_{\mathrm{eff}} = 1$), or turbulent flow ($\varepsilon_{\mathrm{eff}} >> 1$). $\varepsilon_{\mathrm{eff}}$ models the initial cooling in the EWH after a water draw. Note that choosing $\varepsilon_{\mathrm{eff}}$ in a turbulent flow setting has to be done with great care since numerical stability can be compromised when simulating this kind of scenario. Throughout this thesis, a laminar setting for the turbulent mixing coefficient is used ($\varepsilon_{\mathrm{eff}} = 1$).

Equation (2.1) is a standard parabolic PDE with an additional convective term. With the use of the Crank-Nicholson scheme, proposed in [16] and applied by Vrettos et al. [6], equation (2.1) is solved numerically.
With the Crank-Nicholson scheme, we denote the mesh in time with $\triangle t$, and the mesh in space with $\triangle x$.
In addition, to be able to solve (2.1) numerically, two boundary conditions for the top and bottom layer are needed. For this purpose, two artificial layers are regarded: one representing the incoming water temperature to the tank, $T^1 = T_{\mathrm{cw}}$, and the other accounting for ambient temperature, $T^{n+2} = T_{\mathrm{a}}$. Therefore, the actual layers of the EWH range from T^2 to T^{n+1} .
The number of grid points in the space variable x, n, is in our case the number of temperature layers for the EWH. The temperature of layer i at time k is denoted by T_k^i. This discretization of space and time, combined with the boundary conditions allow to express the problem in matrix form:

$$\mathbf{Z}_1\mathbf{T}_{k+1} = \mathbf{Z}_2\mathbf{T}_k + \mathbf{Z}_3 u_k, \tag{2.2}$$

being $\mathbf{T}_k \in \mathbb{R}^{n+2}$ the temperature vector, $u_k \in \{0,1\}$ the binary variable of heating operation (switch ON or OFF; explained later on in Section 2.3), k denotes discretized time, and the matrices $\mathbf{Z}_1$, $\mathbf{Z}_2$ and $\mathbf{Z}_3$ have the following form:

$$\mathbf{Z}_1 = \begin{pmatrix} 1 & 0 & 0 & 0 & 0 & \dots & 0 & 0 & 0 & 0 \\ -4d & \frac{1}{\triangle t} & 0 & 0 & 0 & \dots & 0 & 0 & 0 & -k' \\ 0 & -q_1 & q_2 & q_3 & 0 & \dots & 0 & 0 & 0 & -k \\ \vdots & \vdots & \vdots & \vdots & \vdots & \dots & \vdots & \vdots & \vdots & \vdots \\ 0 & 0 & 0 & 0 & 0 & \dots & -q_1 & q_2 & q_3 & -k \\ 0 & 0 & 0 & 0 & 0 & \dots & 0 & 0 & \frac{1}{\triangle t} & -k' \\ 0 & 0 & 0 & 0 & 0 & \dots & 0 & 0 & 0 & 1 \end{pmatrix}, \tag{2.3}$$

$$\mathbf{Z}_2 = \begin{pmatrix} 1 & 0 & 0 & 0 & 0 & \dots & 0 & 0 & 0 & 0 \\ 0 & q_5 & e & 0 & 0 & \dots & 0 & 0 & 0 & 0 \\ 0 & q_1 & q_4 & -q_3 & 0 & \dots & 0 & 0 & 0 & 0 \\ \vdots & \vdots & \vdots & \vdots & \vdots & \dots & \vdots & \vdots & \vdots & \vdots \\ 0 & 0 & 0 & 0 & 0 & \dots & q_1 & q_4 & -q_3 & 0 \\ 0 & 0 & 0 & 0 & 0 & \dots & 0 & q_6 & q_5 & 0 \\ 0 & 0 & 0 & 0 & 0 & \dots & 0 & 0 & 0 & 1 \end{pmatrix}, \tag{2.4}$$

$$\mathbf{Z}_3 = \begin{pmatrix} 0 & \dots & 0 & \frac{\eta P_{\text{el}}}{m_i c} & 0 & \dots & 0 \end{pmatrix}. \tag{2.5}$$

In matrices $\mathbf{Z}_1$, $\mathbf{Z}_2$, $\mathbf{Z}_3$ the following definitions are needed: $e \doteq \frac{a\varepsilon_{\text{eff}}}{\triangle x^2}$, $d \doteq \frac{V}{4\triangle x}$, $q_1 \doteq \frac{e}{2} + d$, $q_2 \doteq \frac{1}{\triangle t} + e + \frac{\tilde{k}}{2}$, $q_3 \doteq d - \frac{e}{2}$ and $q_4 \doteq \frac{1}{\triangle t} - e - \frac{\tilde{k}}{2}$.
$\tilde{k}'$ is the heat loss coefficient of the top and bottom layers, and $\tilde{k}' > \tilde{k}$ due to the larger heat loss area of these layers. P_{el} is the nominal electric power of the heating element, η is the electrical efficiency coefficient, m^i is the water mass of layer i, and c is the specific heat capacity of water.
The structure of equation (2.5) shows that only one layer was assumed as the heating zone. Of course, this definition could be adapted to larger heating zones, by including more non-zero entries in vector $\mathbf{Z}_3$.

Since matrix $\mathbf{Z_1}$ is non-singular by construction, equation (2.2) can be rewritten as

$$\mathbf{T}_{k+1} = \mathbf{A}_k \mathbf{T}_k + \mathbf{B}_k u_k, \tag{2.6}$$

where $\mathbf{A}_k = \mathbf{Z}_1^{-1}\mathbf{Z}_2$ and $\mathbf{B}_k = \mathbf{Z}_1^{-1}\mathbf{Z}_3$. All in all, equation (2.6) results in a linear time-varying (LTV) system, which characterizes the temperature evolution of the EWH tank with high precision.

2.2 Modeling of natural convection

Natural convection is a type of heat transport, in which the fluid motion is not generated by any external source, but by density differences in the fluid, occurring due to temperature gradients. The effect of natural convection is that of two opposing forces: buoyant force F^b for warmer water layers, and viscous force F^v, which accounts for friction that opposes the fluid motion.
In addition, the density of each water layer i, ρ^i, has to be calculated.

The buoyant forces for each water layer i ,$F^{b,i}$, are obtained with the equation

$$F^{b,i} = \min \left\{ 0, g m^i \frac{\rho_{\text{ref}} - \rho^i}{\rho_{\text{ref}} + \rho^i} \right\}, \tag{2.7}$$

where ρ_{ref} is the minimum between the average density of the water layers above i and density ρ^{i+1}, m^i is the water mass of layer i, and g is the gravitational constant.

The viscous forces for each water layer i, $F^{v,i}$, can be calculated using the velocities from the previous time step for each layer, U^i, according to

$$F^{v,i} = -bU^i. \tag{2.8}$$

The parameter b of equation (2.8) depends on the water viscosity and the geometry of the tank.

Based on these two forces and applying Newton's law of motion, we calculate the acceleration of each water layer. This gives the displacement $\triangle i$ for each water layer i, which determines the temperature mixing between layers:

$$T^j = rT^{j+1} + (1-r)\,T^j, \text{ for } j \in [i, i+\triangle i]\,, \tag{2.9}$$

where $r \in [0,1]$ is the mixing ratio. The value $r = 0$ assumes no mixing and $r = 1$ assumes absolute mixing with the adjacent layer.
The parameters b and r can be identified from experimental results. In this thesis the values from Vrettos et al.'s TABLE I [6] will be used, where $b = 1\left[\frac{\mathbf{kg}}{\mathbf{s}}\right]$ and $r = 0.7\,[-]$.
In the end, the changes in temperature produced by natural convection are added to the changes in temperature from the system dynamics from Section 2.1.

2.3 Internal thermostat controller

At this point, and to review the theory introduced in Sections 2.1 and 2.2, there are some distinctions to make between the different layers of the EWH:

- **Regular layers** $\left(\left[T^2, \ldots, T^{n+1}\right] \setminus \left[T^1_{n_{\text{heat}}}, \ldots, T^l_{n_{\text{heat}}}\right]\right)$: they exchange heat and mass with the adjacent layers (above and below). They also dissipate

some heat through the side of the tank.

- **Heating element layers** $\left(\left[T^1_{n_{\text{heat}}}, \ldots, T^l_{n_{\text{heat}}}\right]\right)$: in addition to the properties for regular layers, these layers are assumed to be affected by the heating element. The heat input occurs once the heating element is turned ON (also introducing a large amount of turbulence and mix).

  For this project, it will assumed that there is only one layer with heating element (instead of l different ones), denoted with $T_{n_{\text{heat}}}$.

- **Bottom layer** $\left(T^1\right)$: the bottom layer exchanges heat and mass with the layer above. It also dissipates heat through the bottom and the side wall of the tank. In addition, it receives the cold water from the inlet, whenever the tank is re-filled with cold water.

- **Top layer** $\left(T^{n+2}\right)$: the top layer exchanges heat and mass only with the adjacent bottom layer, and it also loses heat to the ambience through the top and the side of the tank.

Each EWH has a thermostat, usually built into the heating element layer n_{heat}. This device greatly influences the evolution of the power demand for the EWH. The main function of the internal thermostat is to turn the heating element ON and OFF, depending on the measured internal temperature of the tank.
Assuming we have an EWH denoted with ϑ, the rule for the internal binary controller can be described as

$$u^{\vartheta}(k) = \begin{cases} 0 & , \text{ if } T^{\vartheta}_{n_{\text{heat}}}(k) \geq T^{\vartheta}_{\max} \\ 1 & , \text{ if } T^{\vartheta}_{n_{\text{heat}}}(k) \leq T^{\vartheta}_{\min} \\ u^{\vartheta}(k-1) & , \text{ if } T^{\vartheta}_{\min} < T^{\vartheta}_{n_{\text{heat}}}(k) < T^{\vartheta}_{\max} \end{cases}, \tag{2.10}$$

where $u^{\vartheta}(k) \in \{0,1\}\ \forall k$ is the internal control signal for the heating element, $T^{\vartheta}_{n_{\text{heat}}}(k)$ is the temperature at the heating element layer at time step k, and $T^{\vartheta}_{\min}$ and $T^{\vartheta}_{\max}$ are the lower and upper temperature thresholds of the temperature deadband δ^{ϑ}.
As can be seen from the definition (2.10), the command is to switch the EWH OFF, if the temperature $T^{\vartheta}_{n_{\text{heat}}}(k)$ exceeds $T^{\vartheta}_{\max}$ or switch the EWH ON if the temperature $T^{\vartheta}_{n_{\text{heat}}}(k)$ is below $T^{\vartheta}_{\min}$. On the other hand, if the temperature $T^{\vartheta}_{n_{\text{heat}}}(k)$ is within the deadband δ^{ϑ}, the control state from the previous time step, $u^{\vartheta}(k-1)$, is keeped.

2.4 Describing the stochastic water draws

The water draws are due to the household consumer behaviour. Whenever a consumer needs warm water, a water draw is placed, altering the temperature and dynamics of his EWH.
In the eyes of the grid operator, these water draws occur randomly. However, there are some patterns that can be studied from a statistical standpoint.
The proposed scheme to model the water draws involves using a random value for: draw starting time, draw duration, and flow rate.
The following steps describe the construction of a water draw realization for a day:

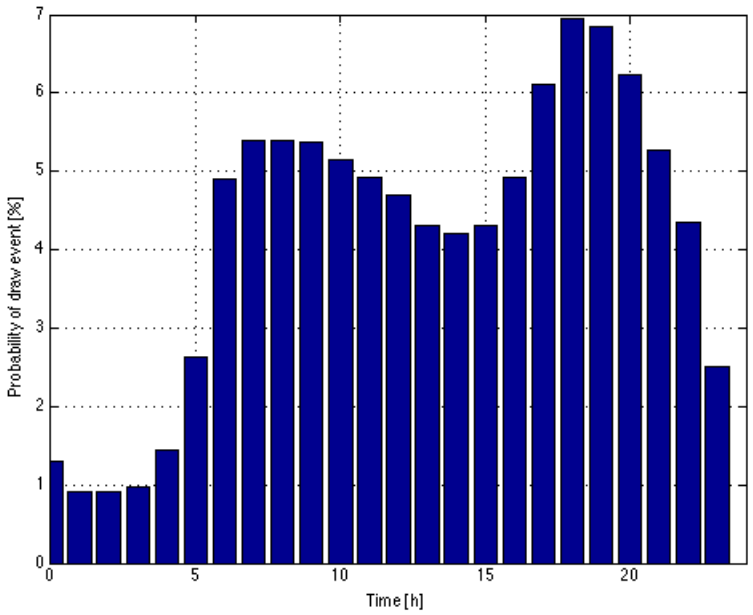

Figure 2.1: Profile from the probability of a water draw during the day

1. First, the probability of a draw event p_{draw} is taken from the profile presented by Lutz [17]. This was a report for the California Energy Comission, and its resulting profile is depicted in Figure 2.1.

2. The total number of water draws per day is determined from an uniform distribution,
$$n_{\text{daily}} \sim \text{Unif}\left(\underline{n_{\text{daily}}}, \overline{n_{\text{daily}}}\right). \tag{2.11}$$

3. The hourly averaged draw probability, $n_{\text{hourly}}^{\text{ave}}$, is the product between p_{draw} and n_{daily}.

4. Next, the vector of time instants when a draw takes place has to be constructed. Lets call this vector $\mathbf{t}_{\text{draw}}$. $\mathbf{t}_{\text{draw}}$ is the cumulative sum of the vector of intervals between water draw events, $\triangle\mathbf{t}_{\text{draw}}$. For the course of a day, $\triangle\mathbf{t}_{\text{draw}}$ can be computed using an exponential distribution with parameter $\frac{1}{n_{\text{daily}}^{\text{ave}}}$:
$$\triangle\mathbf{t}_{\text{draw}} \sim \text{Exp}\left(\frac{1}{n_{\text{daily}}^{\text{ave}}}\right). \tag{2.12}$$

5. The draw duration times are assembled in the vector $\triangle\mathbf{t}_{\text{duration}}$.

   For this, the consumer's draws of hot water can be divided into different categories. We define a peak period of the day (between the hours 7 and 23), during which any draw is assumed to be a shower $T_{\text{draw}}^{\text{long}}$ or a medium load $T_{\text{draw}}^{\text{medium}}$, with a probability of 30% or a short load $T_{\text{draw}}^{\text{short}}$ with a probability of 70%. During the peak period, and if a water draw is either a shower or a medium load, then it is a shower with 14% probability, and a medium load with 86% probability.

6. To induce a variation of flow rates, we draw a normalized flow rate from a normal distribution, with standard deviation $\sigma_{m_{\text{draw}}}$ and mean μ, for every draw event:
$$\dot{\mathbf{m}}_{\text{draw}} \sim \mathcal{N}\left(\mu, \sigma_{\dot{m}_{\text{draw}}}^2\right). \tag{2.13}$$

7. From the information contained in the three vectors $\mathbf{t}_{\text{draw}}$, $\dot{\mathbf{m}}_{\text{draw}}$ and $\triangle\mathbf{t}_{\text{duration}}$, the normalized mass flow time series $\dot{m}_{\text{norm}}$ can be assembled. The draw time series is consequently scaled to equal the daily water usage m_{daily}.

In Figure 2.2 an example of a water draw realization is shown to illustrate the described construction method. Note that the draw profile is shown for the duration of an entire day, and for only one EWH.

On the upper subplot, in the earliest hours of the day (between hours 0 and 5) there are almost no water draws. Then some draws are placed during the day, peaking in the afternoon (heavier use, with showering and cooking), and dropping again in the last hours of the day. On the lower subplot, the total water draw flow can be seen.

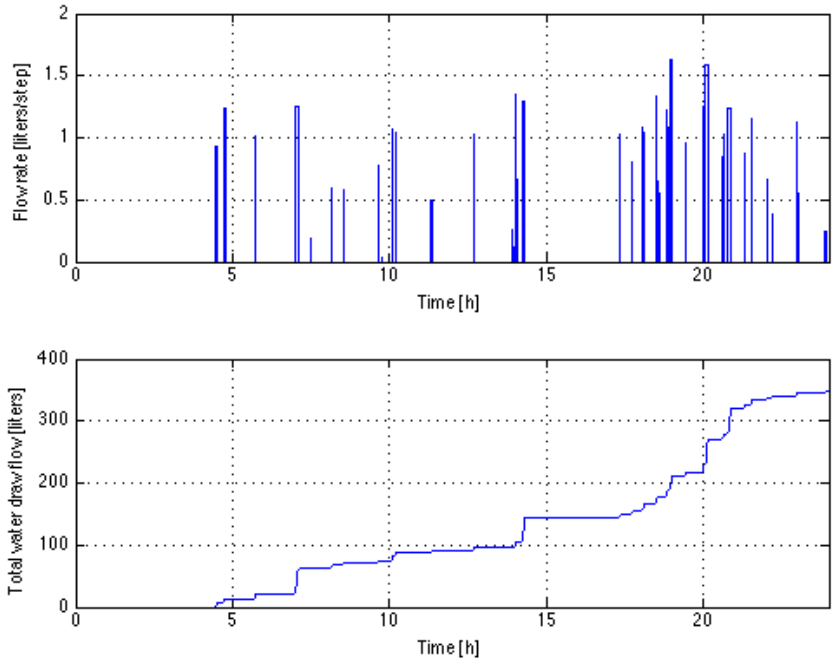

Figure 2.2: Profile from the probability of a water draw during the day

Parameters for the water draws

Table 2.1 shows the values for the parameters needed to model the water draws. The column **Distribution** denotes Unif as the uniform distribution and $\mathcal{N}$ as the normal distribution.

It is important to note that the row for the number of draws per day is dependant on the capacity of the tank, as explained in Section 3.1. For the volume vector

Vol $= \{100, 200, 300, 400\}$ [liters] the boundaries for the uniform distribution for the number of draws per day are:

$$\begin{aligned} \underline{\mathbf{n}_{\text{daily}}} &= \{10, 20, 30, 30\} \\ \overline{\mathbf{n}_{\text{daily}}} &= \{20, 40, 60, 60\} \end{aligned}, \tag{2.14}$$

depending on the specific volume of the tank.

Meaning	Symbol	Distribution	Values	
Number of draws per day	n^j_{daily}	Unif	$\underline{n_{\text{daily}}} \in \underline{\mathbf{n}_{\text{daily}}}$	$\overline{n_{\text{daily}}} \in \overline{\mathbf{n}_{\text{daily}}}$
Long water draw duration	$T^{\text{long}}_{\text{draw}}$	$\mathcal{N}$	$\mu = 5$ [min]	$\sigma = 1$ [min]
Medium water draw duration	$T^{\text{medium}}_{\text{draw}}$	$\mathcal{N}$	$\mu = 1$ [min]	$\sigma = 6$ [s]
Short water draw duration	$T^{\text{short}}_{\text{draw}}$	$\mathcal{N}$	$\mu = 1$ [min]	$\sigma = 6$ [s]
Hot water flow rate (long)	$\dot{m}^{\text{long}}_{\text{draw}}$	$\mathcal{N}$	$\mu = 8$ $\left[\frac{\text{liters}}{\text{min}}\right]$	$\sigma = 1$ $\left[\frac{\text{liters}}{\text{min}}\right]$
Hot water flow rate (medium)	$\dot{m}^{\text{medium}}_{\text{draw}}$	$\mathcal{N}$	$\mu = 6$ $\left[\frac{\text{liters}}{\text{min}}\right]$	$\sigma = 1$ $\left[\frac{\text{liters}}{\text{min}}\right]$
Hot water flow rate (short)	$\dot{m}^{\text{short}}_{\text{draw}}$	$\mathcal{N}$	$\mu = 1$ $\left[\frac{\text{liters}}{\text{min}}\right]$	$\sigma = 2$ $\left[\frac{\text{liters}}{\text{min}}\right]$
Daily water usage	m_{day}	$\mathcal{N}$	$\mu = 200$ [liters]	$\sigma = 20$ [liters]

Table 2.1: Probabilistic parameters for the water draws

2.5 Parameter selection

The described model for an EWH needs a set of parameters. These have to be determined. In our case they were mostly taken from Vaggelis et al. [6], with some caveats. For example, the inlet water temperature T_{cw} and the ambient temperature T_{a} are chosen differently. The reader is advised to read the values of Table 2.2 on page 14 carefully.

In this case, the parameters were tuned and validated using ten temperature measurements from a cylindrical tank from the Lawrence Berkeley National Laboratory [18]. With the exception of the lowest layer of the tank, T^2, the temperature errors were relatively small (less than 3% Mean Average Percentage Error (MAPE)). The upper tank layers performed best in terms to Root Mean Squared Error (RMSE).

Parameter	Symbol	Value	Unit
Tank parameters			
Volume of the tank	-	190	liters
Height of the tank	-	1.19	m
Nominal electrical power of the heating element	P_{el}	4.1	kW
Efficiency coefficient	η	95	%
Thermodynamic parameters			
Water thermal diffusivity	a	$0.1434 \cdot 10^{-6}$	$\frac{\text{m}^2}{\text{s}}$
Water specific heat capacity	c	4185.5	$\frac{\text{J}}{\text{kg}\cdot\text{K}}$
Tank heat loss coefficient	$\tilde{k}$	$6.3588 \cdot 10^{-7}$	$\frac{1}{\text{s}}$
Tank heat loss coefficient (top and bottow layers)	$\tilde{k}'$	$1.2382 \cdot 10^{-6}$	$\frac{1}{\text{s}}$
Gravitational constant	g	9.81	$\frac{\text{m}}{\text{s}^2}$
Tuning parameters			
Friction parameter	b	1	$\frac{\text{kg}}{\text{s}}$
Mixing ratio	r	0.7	-
Simulation parameters			
Mesh in time (discretization)	$\triangle t$	10	s
Mesh in space (discretization)	$\triangle x$	0.119	m
Number of water layers	n	10	-
Layer with heating device	n_{heat}	2	-
Layer with thermostat	$n_{\text{thermostat}}$	3	-
Inlet water temperature	T_{cw}	10	$^{\text{o}}$C
Ambient temperature	T_{a}	20	$^{\text{o}}$C

Table 2.2: EWH model parameters

2.6 Simulations of an individual EWH

In this Section, we are going to gather all the modeling of the previous Sections of this Chapter, and simulate an EWH for an entire day.
The presence of only internal controllers will pose an autonomous scenario from the point of view of the grid operator.

On the example in Figure 2.3, the values of Table Table 2.2 on page 14 were taking, with the following changes:

- The volume of the tank is 300 [liters], and $P_{\text{el}} = 4$ [kW].
- The temperature deadband is $\delta = 7.8803$ [K] and the set-point temperature $T_{\text{set}} = 56.8239$ [$^{\text{o}}$C].

The top subplot of Figure 2.3 shows the water draws, statistically constructed as described in Section 2.4, in liters per minute for the entire day.
On the next subplot a heatmap of the temperature within the tank is displayed. As can be seen, the temperature of the lower layers strongly decrease whenever a water draw occurs.
On the next subplot, the switch of the internal thermostat controller is shown. The behaviour was explained in Section 2.3, and it switches ON a total of 5 times during the day. This is due to the cooling produced by refilling the tank with cold water after a water draw happened. The ON-time of the individual water heater should be between $10 - 15$ % of the total time.
The last subplot shows the temperature evolution of the layers n_{heat} and $n_{\text{thermostat}}$.

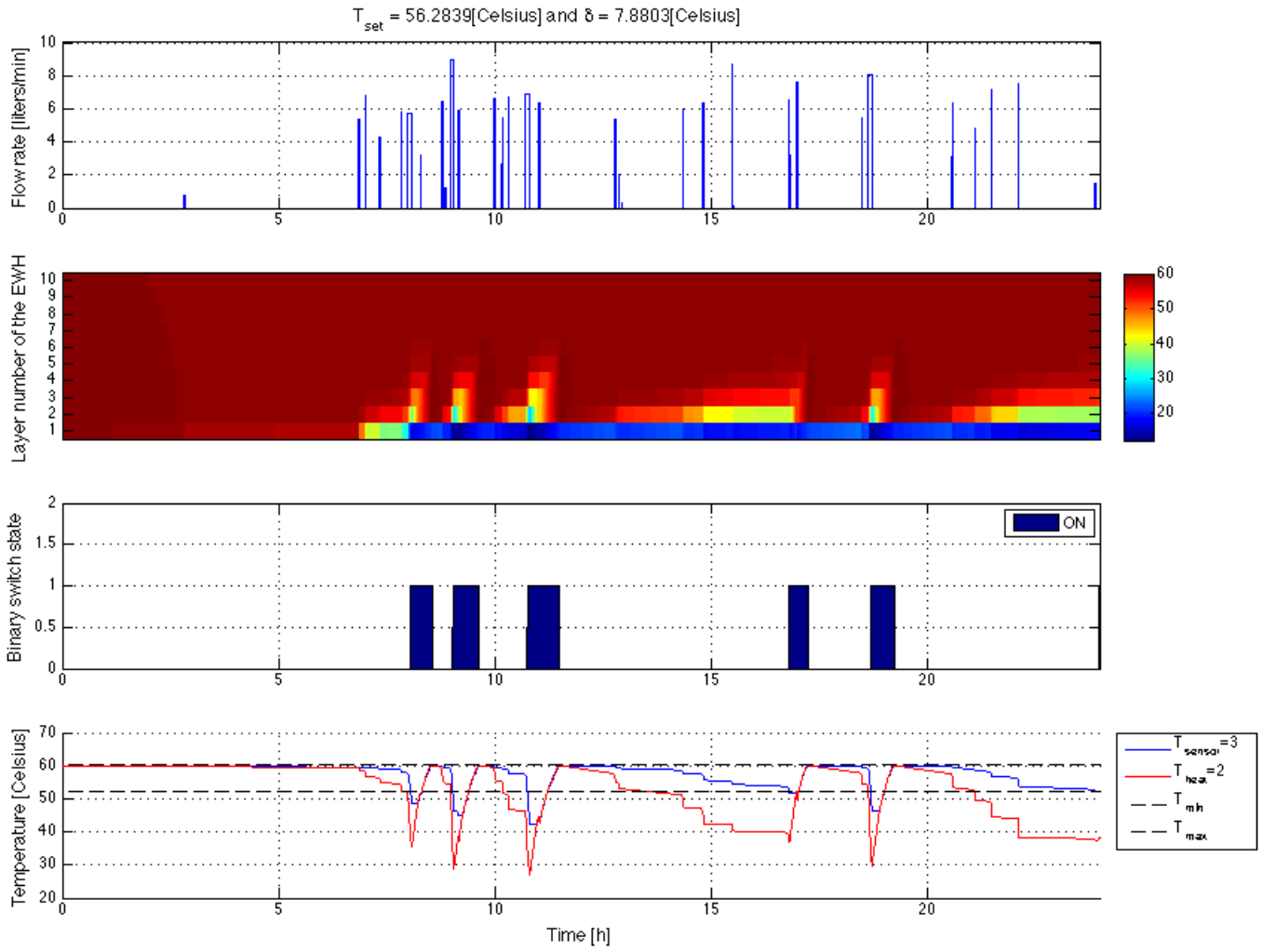

Figure 2.3: Temperature heatmap for one EWH during one day

Chapter 3

Load population model

In this Chapter, the model for a population of EWHs will be developed. In our case, the population will be modeled through statistical distributions for the main tank parameters. This feature adds heterogeneity amongst the TCLs, contrary to homogeneity, where all the parameters are equal for all loads.
For example, Perfumo et al. [1] and Kondoh et al. [5] do an outstanding analysis of a homogenous population of EWHs. However, this abstraction comes at a cost in model accuracy when compared to the more realistic heterogeneous populations.
The main goal of this model will be to investigate the aggregate power consumption of a large population, both in an autonomous setting and with control from a coordination entity (e.g. the grid operator).
In Section 3.1 the selection of the population parameters will be motivated. In Section 3.2 some simulation results are presented. Section 3.3 presents a characterization of the power baseline. Lastly, Section 3.4 introduces the concept of an external control signal to steer the population's behaviour, showing two standard definitions.

3.1 Selecting the population parameters

Lets assume a population of TCLs $\mathcal{P}$, with $N_{\text{app}} \doteq |\mathcal{P}|$ loads. One of the more realistic assumptions that can be made through the modeling phase for that population is adding a level of heterogeneity. This, as opposed to homogeneity, assumes that some of the parameters of the loads are different across the popu-

lation. For EWHs, this is a realistic assumption since they have different sizes and specifications, and come from a variety of different manufacturers.
Also note that a certain amount of correlation has to be assumed between the parameters, as for example a big EWH is more likely to have a big heating element and a big water draw volume.

A heterogenous set of parameters for an EWH population $\mathcal{P}$ can be seen in Table 3.1. This procedure is described in greater detail by Vrettos et al. [6] and Koch [14], and is summarized here:

- A water mass category vector $\mathbf{m}_{\text{cat}}$ is defined, with different tank sizes. The vector of category shares $\mathbf{p}_{\text{cat}}$ represents the percentage that each category has across $\mathcal{P}$.
- The matrix of rated power per category $\mathbf{P}_{\text{cat}}^{\text{rated}}$ gives column-wise possible electric rated powers for the devices of a category. These values are drawn from a discrete uniform distribution.
- For each EWH category, the total water consumption per day is drawn from a continuous uniform distribution. The boundaries $\left[m_{\text{daily,cat}}^{\text{min}}, m_{\text{daily,cat}}^{\text{max}}\right]$ are given column-wise for each category *cat* of the tank size.
- The center and width of the temperature deadband for each EWH ϑ, $T_{\text{set}}^{\vartheta}$ and δ^{ϑ}, are drawn from continuous uniform distributions with intervals $\left[T_{\text{set}}^{\text{min}}, T_{\text{set}}^{\text{max}}\right]$ and $\left[\delta^{\text{min}}, \delta^{\text{max}}\right]$ respectively.
- The thermal loss coefficient U^{ϑ} is varied from a uniform distribution with boundary values U^{min} and U^{max} for each EWH ϑ.
- Lastly, the initial temperature vector $\mathbf{T}_0$ gives the initial condition, and is assumed equal for all EWH.

Meaning	Symbol	Values
Water mass categories	$\mathbf{m}_{\text{cat}}$	$[100, 200, 300, 400]$ [kg]
Category shares	$\mathbf{p}_{\text{cat}}$	$[20, 30, 30, 20]$ [%]
Rated power per category	$\mathbf{P}_{\text{cat}}^{\text{rated}}$	$\begin{bmatrix} 3 & 3.5 & 4 & 4 \\ 3.5 & 4 & 4.5 & 5 \\ 4 & 4.5 & 5 & 6 \end{bmatrix}$ [kW]
Daily draw bounds per category	$\left[\mathbf{m}_{\text{daily,cat}}^{\min}, \mathbf{m}_{\text{daily,cat}}^{\max}\right]$	$\begin{bmatrix} 30 & 50 & 100 & 150 \\ 70 & 100 & 220 & 350 \end{bmatrix}$ [kg]
Temperature set-point bounds	$\left[T_{\text{set}}^{\min}, T_{\text{set}}^{\max}\right]$	$[55, 65]$ [°C]
Deadband size bounds	$\left[\delta^{\min}, \delta^{\max}\right]$	$[5, 15]$ [K]
Heat loss coefficient bounds	$\left[U^{\min}, U^{\max}\right]$	$[0.2, 1]$ $\left[\frac{W}{m^2 K}\right]$
Initial temperature vector	$\mathbf{T}_0$	$[10, 60, \ldots, 60, 20]^T$ [°C]

Table 3.1: Parameters used for the EWH population

3.2 Simulation of the population

In the following Section, some simulations for an EWH population $\mathcal{P}$ with N_{app} loads will be shown.
This will constitute an open-loop scenario, without external control from the centralized control entity. However, the internal controllers described in Section 2.3, and the water draws described in Section 2.4, will be present in the simulations. The sampling time will be $T_{\text{sample}} = 10$ [s].

In Figure 3.1 the simulation for a population of $N_{\text{app}} = 1000$ EWHs is shown over the course of a day.
The upper subplot of the figure shows the aggregate water draws for that day in liters per time step.
The lower subplot shows the aggregate power for the EWH population, where the aggregate power at time k, $P_{\text{agg}}(k)$, is defined as

$$P_{\text{agg}}(k) \doteq \sum_{\vartheta=1}^{N_{\text{app}}} u^{\vartheta}(k) \frac{P_{\text{el}}^{\vartheta}}{\eta^{\vartheta}}, \tag{3.1}$$

where $P_{\text{el}}^{\vartheta}$ is the electric power and η^{ϑ} is the efficiency of the ϑ-th EWH, $u^{\vartheta}(k)$ is the internal switch controller state (ON or OFF) for EWH ϑ at time step k. As can be seen on Figure 3.1, the profile for the aggregate power matches that from the water draws. The internal controllers try to match the hot water

demand and to keep the water temperature of the tanks high by turning internal switches ON.

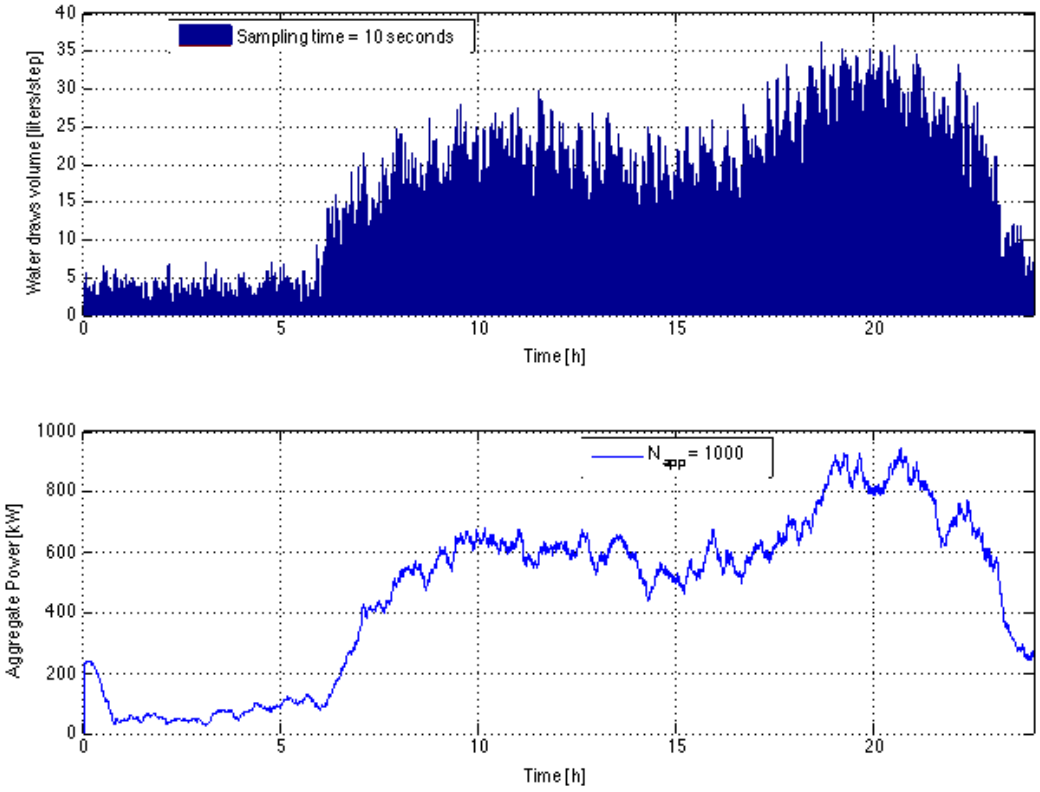

Figure 3.1: Simulation example for $N_{\text{app}} = 1000$ EWHs

3.3 Baseline characterization

Next, an outline of the choice of the number of EWHs N_{app} for the population $\mathcal{P}$ will be presented.
Lets assume a varying population of $N_{\text{app}} = \{1, 10, 100, 1000\}$ EWHs, with autonomous mode (no external control signal, $\hat{u} = 0$), but internal controllers as described in Section 2.3. To get some statistical intuition about the importance of N_{app} in the simulations, $N_E = 20$ different simulations will be made, to get mean $\mu_{N_{\text{app}}}(k)$ and standard deviation $\sigma_{N_{\text{app}}}(k)$ of the aggregate power (3.1). At this point, and to get a more reasonable comparison, the aggregate power should be normalized:

$$\tilde{P}_{\text{agg}}(k) \doteq \frac{P_{\text{agg}}(k)}{\sum_{\vartheta=1}^{N_{\text{app}}} \frac{P_{\text{el}}^{\vartheta}}{\eta^{\vartheta}}}, \tag{3.2}$$

by the power of the population, with $\tilde{P}_{\text{agg}}$ denoting the normalized aggregate power.

Figure 3.2 shows the mean $\mu_{N_{\text{app}}}$ and standard deviation $\sigma_{N_{\text{app}}}$ of the normalized aggregate power $\tilde{P}_{\text{agg}}$ for different values of $N_{\text{app}} \in \{1, 10, 100, 1000\}$.
Also, Figure 3.3 shows the standard deviations $\sigma_{N_{\text{app}}}$ (on the y-axis) for the different number of loads N_{app} along the duration of the day.
As can be seen, the standard deviation decreases as the population size N_{app} increases.
Therefore, it will be necessary for future Chapters to select a population that has a good trade-off between low standard deviation $\sigma_{N_{\text{app}}}$ and low computational time (which is given by the number of loads N_{app}).

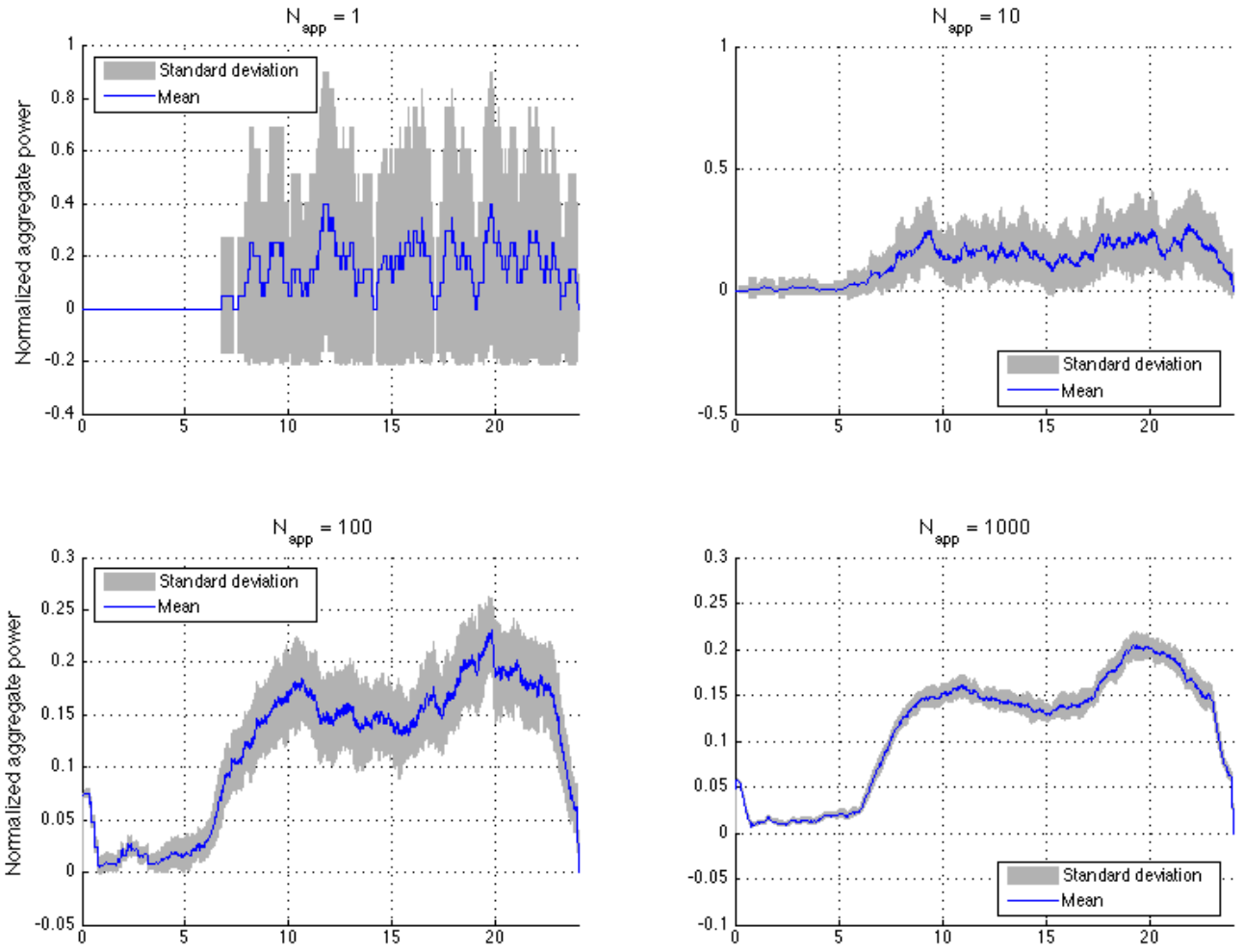

Figure 3.2: Examples for different N_{app} populations average and standard deviation

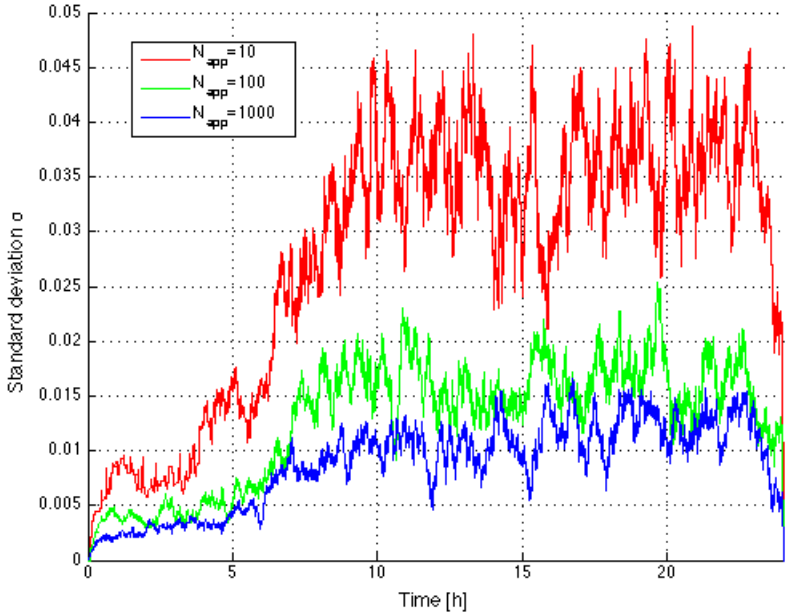

Figure 3.3: Simulation example for $N_{\text{app}} = 1000$ EWHs

Lastly, an analysis of the usage of the EWHs across the population for water draws as described in Section 2.4 will be performed, in terms of internal switch state u^{ϑ}.
The average ON-time of an individual water heater throughout the day is $10-11\%$ of the total time, with a standard deviation of close to 5%. Some simulation results supporting this can be seen on Table 3.2, where every row corresponds to a different population $\mathcal{P}_1, \ldots, \mathcal{P}_5$ of $N_{\text{app}} = 1000$ EWHs, constructed as described in Section 3.1.

Also, Figure 3.4 shows for a population of $N_{\text{app}} = 1000$ EWHs the averaged, maximum and minimum values for the N_{ON} set, over $N_E = 20$ simulations.
Under baseline assumptions the maximal number of EWHs that will be ON at any given time is around 22%, and the average at 20%. This result leaves a majority of the EWHs in the N_{OFF} set, where they can be turned ON by

external control.

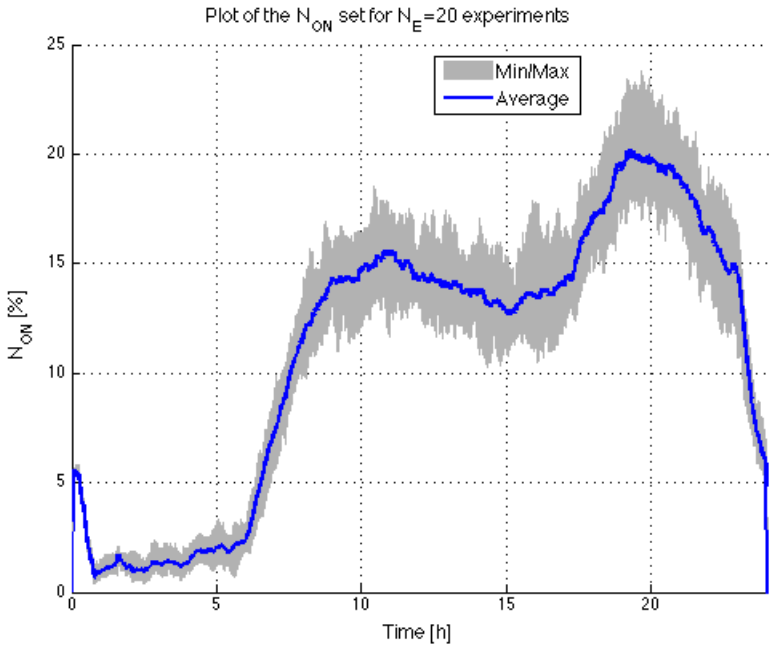

Figure 3.4: Average, maximum and minimum for the N_{ON} set

Population	**Average [%]**	**Standard deviation [%]**
$\mathcal{P}_1$	11.1861	5.2005
$\mathcal{P}_2$	10.9897	4.7445
$\mathcal{P}_3$	10.9805	4.89
$\mathcal{P}_4$	11.0975	4.9332
$\mathcal{P}_5$	11.341	5.1311

Table 3.2: Average time for a single EWH to be ON through different simulations

3.4 External control signal

In this Section, we present two different control strategies to coordinate a population of EWHs. The main objective will be to track a time-varying reference aggregate power signal.
The plant to be controlled will be a population $\mathcal{P}$ with N_{app} EWHs, with population model parameters as introduced in Section 3.1.
Next, two different approaches will be presented: probability switching and temperature set-point variation.

3.4.1 Probabilistic switching

One of the possible controllers to be implemented in the system is probabilistic switching.
The external input at time k will be an uniformly distributed random number, $\hat{u}(k) \sim \text{Unif}(-1, 1)$, which is then broadcasted to all EWHs. Then, each EWH $\vartheta \in \{1, \ldots, N_{\text{app}}\}$ draws an uniformly distributed random number $\xi^{\vartheta}(k) \sim \text{Unif}(0, 1)$, and compares it to the broadcasted value $\hat{u}(k)$. Based on the comparison between these numbers, a switching of the internal thermostat controller $u^{\vartheta}(k)$ takes place or not.

Next, the idea behind Algorithm 3.1 will be explained.
If the external controller signal is positive, with $\hat{u}(k) > 0$, and the drawn number for EWH i is smaller than it, $\xi^{\vartheta}(k) \leq \hat{u}(k)$, then the internal controller is switched ON.
On the other hand, if the external controller signal is negative, with $\hat{u}(k) < 0$, and the drawn number for EWH i is bigger than it, $\xi^{\vartheta}(k) \geq \hat{u}(k)$, then the internal controller is switched OFF.
An additional requirement for the probability switching method is that the temperature of the EWH ϑ is within its temperature deadband: $T^{\vartheta}_{n_{\text{heat}}}(k) \in \delta^{\vartheta}$.
In both cases, the external controller has priority over the internal controller.
This external control structure is usually used in Markov-chain structures, as for example by Koch, Mathieu, Callaway [8, 12]. In this case, the Markov transition matrix describes the probability of TCLs moving from one state bin to another. For this scenario probability switching methods are very common.

Algorithm 3.1 Probabilistic switching method

for $\vartheta = 1, ..., N_{\text{app}}$ **do**
  if $\left(\xi^{\vartheta}(k) \leq \hat{u}(k) \wedge \hat{u}(k) > 0 \wedge T^{\vartheta}_{n_{\text{heat}}}(k) \in \delta^{\vartheta}\right)$ **then**
    $u^{\vartheta}(k) := 1$
  end if
  if $\left(-\xi^{\vartheta}(k) \geq \hat{u}(k) \wedge \hat{u}(k) < 0 \wedge T^{\vartheta}_{n_{\text{heat}}}(k) \in \delta^{\vartheta}\right)$ **then**
    $u^{\vartheta}(k) := 0$
  end if
end for

Figure 3.5 shows two examples for probability switching for the hourly interval $\mathrm{I} = [18, 19]$ [hour].
On the left column, a positive external input of $\hat{u} = 0.3$ is applied for 10 minutes. On the right column it is a negative input of $\hat{u} = -0.5$, also lasting 10 minutes. The lower row shows in blue the normalized aggregate power $\tilde{P}_{\text{agg}}$ of the baseline (autonomous setup with $\hat{u}(k) = 0, \forall k \in \mathrm{I}$), and in red the normalized aggregate power $\tilde{P}_{\text{agg}}$ resulting from applying the external input.
The first and more important observation that can be made is that the baseline level plays a crucial role.

As discussed at the end of Section 3.3, for a population of $N_{\text{app}} = 1000$ EWHs in autonomous mode, the subset of EWHs that are on N_{ON} is low during the entire day. There is a high power reserve when sending a positive probability switching signal $\hat{u} > 0$ as basically the set relationship $N_{\text{OFF}} \gg N_{\text{ON}}$ gives a higher margin to switch EWHs ON. This can be seen from the amplitudes of Figure 3.5 for $\tilde{P}_{\text{agg}}$, where when applying the input of $\hat{u} = 0.3$ the normalized aggregate power increases to above 0.5. On the other hand, when applying the negative input $\hat{u} = -0.5$.

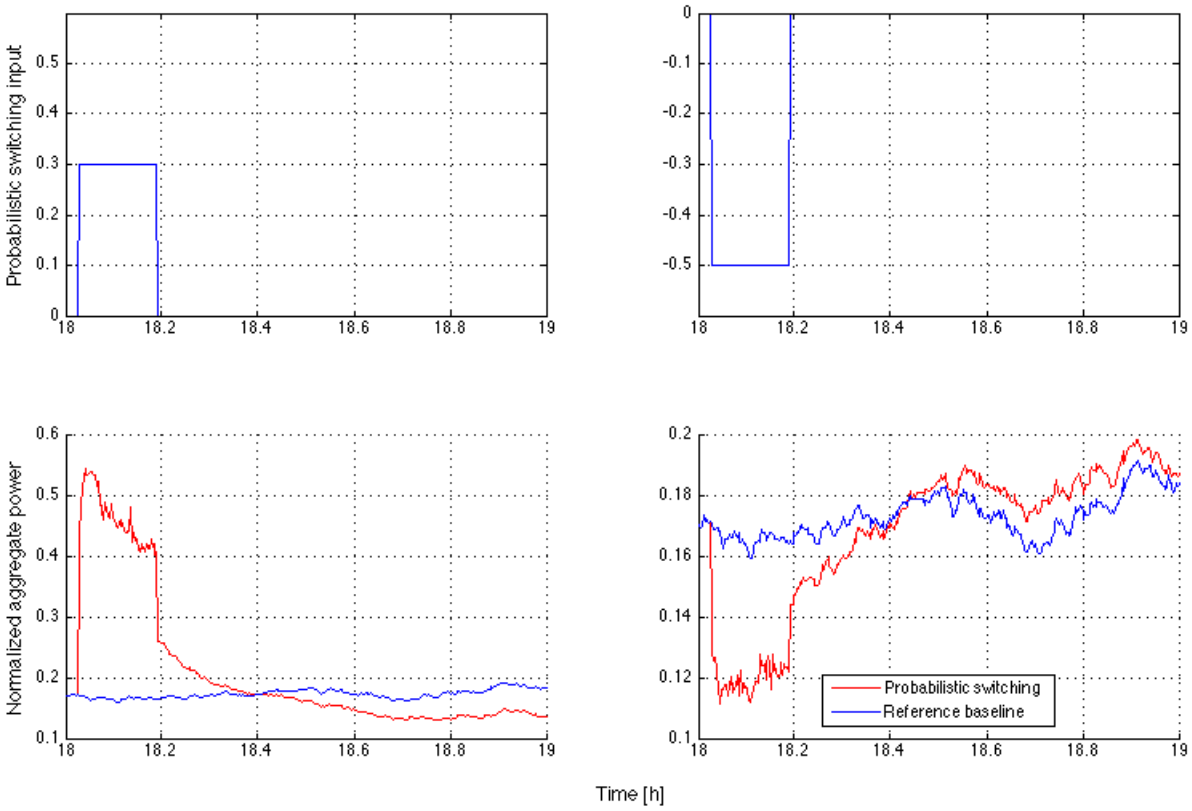

Figure 3.5: Probability switching examples for $\hat{u} = 0.3$ and $\hat{u} = -0.5$ pulses

3.4.2 Temperature set-point variation

A slightly different approach for the external controller consists on varying the set-point temperature $T^{\vartheta}_{\text{set}}$ of all EWHs.

In this case, the external controller draws a uniformly distributed random number $\hat{u}(k) \sim \text{Unif}(-1, 1)$ whenever a deviation from the aggregate power baseline is needed. This is called an event.

Then, the set-point temperature, $T^{\vartheta}_{\text{set}}$, and the maximal and minimal temperatures, $T^{\vartheta}_{\text{max}}$ and $T^{\vartheta}_{\text{min}}$, are recalculated for all EWHs $\vartheta \in \{1, \ldots, N_{\text{app}}\}$ as follows in Algorithm 3.2, with δ^{ϑ} as the temperature deaband for EWH ϑ. Therefore, the algorithm shifts the temperature range for all EWHs, which has had an indirect effect on the internal controllers of each EWH ϑ. This causes indirect ON switching when $\hat{u} > 0$ and indirect OFF switching when $\hat{u} < 0$.

Let us look at the following example with N_{app} EWHs, whose temperature deadband were $\delta^{\vartheta} = 10$ [°C] $\forall \vartheta \in \{1, \ldots, N_{\text{app}}\}$, and the minimum and maximum temperatures were $T^{i}_{\min} = 55$ [°C] and $T^{\vartheta}_{\max} = 65$ [°C], $\forall \vartheta \in \{1, \ldots, N_{\text{app}}\}$ respectively. Assuming that the external input signal, $\hat{u}(k) = 0.1$ was sent at time step k, then the new limits would be 56 and 66 [°C]. This change would have as a consequence that all the EWHs whose temperature are between 55 [°C] and 56 [°C] would be automatically switched ON by the internal controllers. On the other hand, EWHs which were going to be switched OFF because of surpassing the old $T_{\max} = 65$ [°C] will continue heating water until they hit the newer higher limit of 66 [°C].

Algorithm 3.2 Set-point variation method

1: **for** $\vartheta = 1, ..., N_{\text{app}}$ **do**
2: **if** $(\hat{u}(k) > 0)$ **then**
3: $T^{\vartheta}_{\text{set}} := T^{\vartheta}_{\text{set}} + |\hat{u}(k)| \cdot \delta^{\vartheta}$
4: **end if**
5: **if** $(\hat{u}(k) < 0)$ **then**
6: $T^{\vartheta}_{\text{set}} := T^{\vartheta}_{\text{set}} - |\hat{u}(k)| \cdot \delta^{\vartheta}$
7: **end if**
8: $T^{\vartheta}_{\min} := T^{\vartheta}_{\text{set}} - \frac{1}{2}\delta^{\vartheta}$
9: $T^{\vartheta}_{\max} := T^{\vartheta}_{\text{set}} + \frac{1}{2}\delta^{\vartheta}$
10: **end for**

In Figure 3.6, a schematic overview of the temperature set-point variation method is presented.

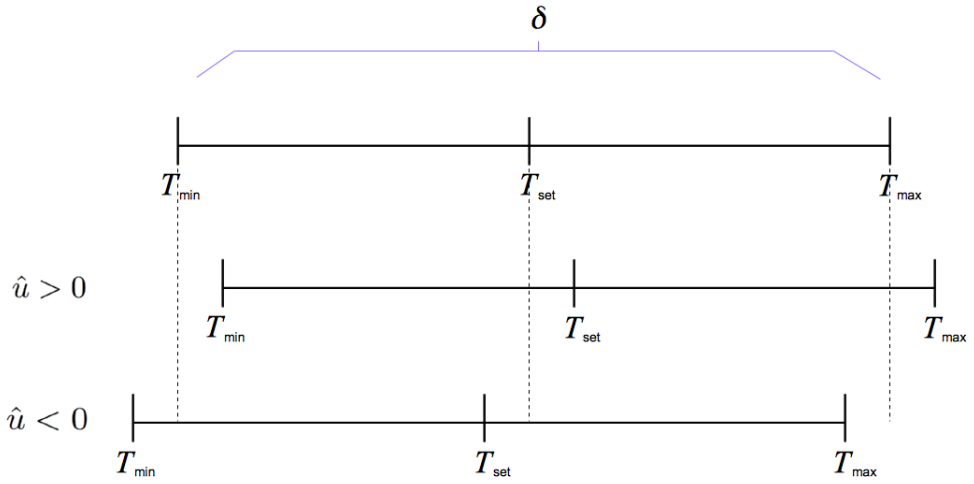

Figure 3.6: Visualization of the set-point variation

Chapter 4

System Identification

In this Chapter, and for the remaining of this thesis, an EWH population $\mathcal{P}$ will be assumed, constructed as described in Chapter 3. The external control method from now on will be temperature set-point variation, as described in Section 3.4.2.
However, it will be also assumed that as grid operators, our knowledge about $\mathcal{P}$ is limited. Following the discussion of Section 3.3, for this Chapter we will choose $N_{\text{app}} = 1000$ EWHs as the population size. This choice is a trade-off between small standard deviation in the baseline aggregate power and the computational time for the simulations.
As well as N_{app}, an averaged water draw profile (computed offline) is known, along with the capability to measure the aggregate power consumption for the population under external control.

The objective of this Chapter will be to find a simplified mathematical description of the system using System Identification [19] techniques. Similar approaches can be found in the projects of Callway [10] (for wind power plants) or Perfumo et al. [1] (for populations of ACs).
More importantly, this description should be a simplified model, suitable for use in controller design later on in Chapter 5.

4.1 Signals of interest

In this Chapter the data will be in the discrete time-domain, sampled with period $T_{\text{sample}} = 10$ [s] .
Lets define $\mathcal{U} \doteq [-1, 1] \subset \mathbb{R}$ as the space for the inputs and $\mathcal{Y} \doteq \left[0, \sum_{\vartheta=1}^{N_{\text{app}}} \frac{P_{\text{el}}^{\vartheta}}{\eta^{\vartheta}}\right] \subset \mathbb{R}_+$ as the space for the outputs. The definition of $\mathcal{U}$ comes motivated by the external input signal $\hat{u}$ for temperature set-point variation, and the definition for $\mathcal{Y}$ by the fact that the aggregate power of an EWH population will always be positive and bounded.

The possible external control signals $\hat{u} \in \mathcal{U}$ will be the ones described for temperature set-point variation, as explained in Section 3.4.2.

For the output signal $y \in \mathcal{Y}$, we are going to use the following definition:

$$y \doteq y_{\text{measured}} - y_{\text{baseline}}^{\text{ave}}, \tag{4.1}$$

where $y_{\text{baseline}}^{\text{ave}}$ is the averaged baseline for aggregate power consumption in the autonomous case (with $\hat{u} = 0$), and y_{measured} is the aggregate power measured for the population in open-loop, with external control ($\hat{u} \neq 0$) .
The baseline consumption $y_{\text{baseline}}^{\text{ave}}$ addresses the case described in Section 3.3, and is computed offline. The idea is to average $N_E = 20$ autonomous experiments for the population $\mathcal{P}$ to get the signal $y_{\text{baseline}}^{\text{ave}}$.
In addition, the output y is going to be normalized by the total power of the entire population. Defining $\tilde{\mathcal{Y}} \subset [-1, 1]$, this normalized signal denoted with $\tilde{y} \in \tilde{\mathcal{Y}}$ is constructed as

$$\tilde{y} \doteq \frac{y_{\text{measured}} - y_{\text{baseline}}^{\text{ave}}}{\sum_{\vartheta=1}^{N_{\text{app}}} \frac{P_{\text{el}}^{\vartheta}}{\eta}}, \tag{4.2}$$

where $\sum_{\vartheta=1}^{N_{\text{app}}} \frac{P_{\text{el}}^{\vartheta}}{\eta}$ is the total power that can be achieved by the population, when all the EWHs are active in the ON state.

The last signal that will be discussed is an averaged water draw profile. This signal will be treated as an exogenous input for the system and is also previously computed.

Recalling the theory of Section 2.4, the signal w^{ave} is obtained as follows:

$$w^{\text{ave}}(k) = \frac{1}{N_E} \sum_{i=1}^{N_E} w_i(k), \tag{4.3}$$

where N_E are the number of experiments, k denotes the discrete time index, w_i is the random water draw of experiment i, and w^{ave} is the averaged water draw profile.
The signal w^{ave} belongs to the space $\mathcal{W} \doteq [0, w^{\text{ave}}_{\max}] \subset \mathbb{R}_+$, which is also compact and bounded.

In Figure 4.1, an averaged water draw profile in $\left[\frac{\text{liters}}{\text{min}}\right]$ can be seen for $N_E = 20$ experiments. The blue line is the averaged profile w^{ave}, and the grey-shaded area is the standard deviation out of the N_E experiments.

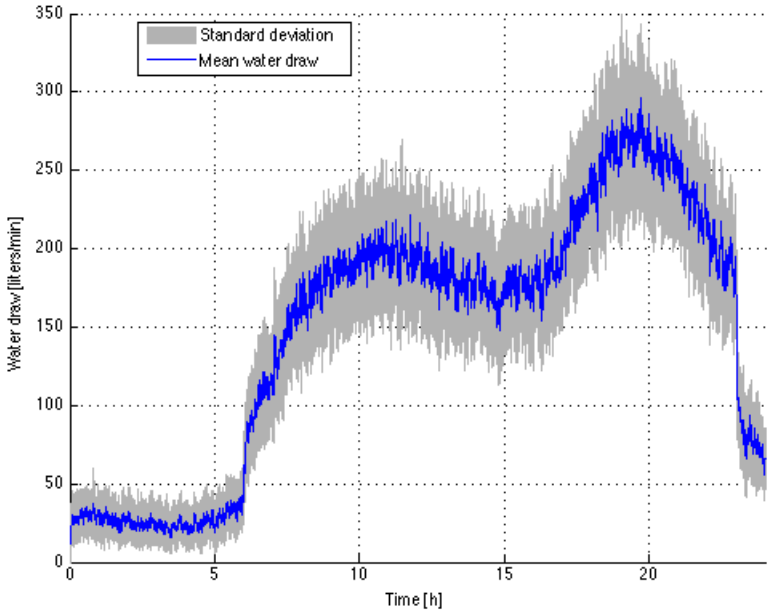

Figure 4.1: Averaged water draw profile

4.2 System properties

Our main goal is to find a function

$$\begin{array}{rcl} \gamma : \mathcal{U} \times \mathcal{W} & \rightarrow & \tilde{\mathcal{Y}} \\ (\hat{u}, w^{\text{ave}}) & \mapsto & \gamma\left(\hat{u}, w^{ave}\right) = \tilde{y} \end{array}, \tag{4.4}$$

for $\hat{u} \in \mathcal{U}$, $w^{\text{ave}} \in \mathcal{W}$ and $\tilde{y} \in \tilde{\mathcal{Y}}$, such that the input-output relationship between the external input $\hat{u}$ and the output $\tilde{y}$ is characterized. An approach on this characterization will be presented in Section 4.3.

The most important system properties that should be investigated are:

1. **Linearity**: the function $\gamma : \mathcal{U} \times \mathcal{W} \rightarrow \tilde{\mathcal{Y}}$ is called linear if and only if $\forall \hat{u}_1, \hat{u}_2 \in \mathcal{U}$, $w^{\text{ave}} \in \mathcal{W}$, $\beta_1, \beta_2 \in \mathcal{B}$

$$\gamma\left(\alpha_1 \hat{u}_1 + \alpha_2 \hat{u}_2, w^{\text{ave}}\right) = \beta_1 \cdot \gamma\left(\hat{u}_1, w^{\text{ave}}\right) + \beta_2 \cdot \gamma\left(\hat{u}_2, w^{\text{ave}}\right). \tag{4.5}$$

   In Appendix A, some examples to check the linearity property can be seen.

   The main conclusion that can be drawn from those examples is that the system is not linear. One of the reasons is because the definition for the output $\tilde{y}$ (4.2) contains the baseline signal $y^{\text{ave}}_{\text{baseline}}$.

   If both external inputs $\hat{u}_1$, $\hat{u}_2$ have the same sign (either positive or negative), then linearity could be assumed under some accuracy losses.

2. **Time invariance**: an additional important feature for the function $\gamma : \mathcal{U} \times \mathcal{W} \rightarrow \tilde{\mathcal{Y}}$ is its time dependancy. Lets regard equation (4.4) with the discrete time variable k.

   The function (4.4) is called time varying if

$$\tilde{y}\left(k\right) = \gamma\left(\hat{u}\left(k\right), w^{\text{ave}}\left(k\right), k\right), \tag{4.6}$$

   and time invariant if $\tilde{y}\left(k\right) = \gamma\left(\hat{u}\left(k\right), w^{\text{ave}}\left(k\right)\right)$, where k is the discrete time variable. Note that in the latter, the function γ does not depend directly on time k.

   Therefore, the system is time invariant if the response to a certain external input signal does not depend on absolute time.

Examining the population of loads in the ON state N_{ON}, displayed on Figure 3.4, already gives a pointer towards the fact that the system is highly time dependant.

Lets assume that we examine the following two time intervals of the day: $\mathrm{I}_4 = [4, 5]$ [hour] and $\mathrm{I}_{18} = [18, 19]$ [hour].
Lets assume that the external input $\hat{u}(k) = 0.3$ is applied for the first 10 minutes of the time intervals I_1 and I_2, and then recovered to $\hat{u}(k) = 0$ for the remaining time:

$$\hat{u}(k) = \begin{cases} 0.3 & , \ 0 \text{ [min]} \leq \mathrm{I}_i(k) \leq 10 \text{ [min]} \\ 0 & , \ \mathrm{I}_i(k) > 10 \text{ [min]} \end{cases} , \ i = 1, 2. \tag{4.7}$$

Figure 4.2 shows the simulation of such a scenario for a population $\mathcal{P}$ of $N_{\mathrm{app}} = 1000$ EWHs.
The upper row subplots show the external input profile $\hat{u}$, starting at the beginning of intervals I_1 and I_2.
The lower row subplots show the normalized aggregate power signal $\tilde{y}$.
As is clear from the signal levels in the resulting output $\tilde{y}$, for interval I_1 the output achieves a maximal value close to 0.6, whereas the output for interval I_2 only achieves a maximal value of 0.4.
This counterexample clearly shows that the system at hand is time varying.

The reason for the time variance is mainly the water draw profile. The aggregate power baseline y_{baseline} that results from the draws, and the resulting sets N_{ON} and N_{OFF} account for this time dependency. As the output signal $\tilde{y}$ subtracts the baseline from the measurement, the output is going to depend on the fluctuations resulting from the baseline, as depicted in Section 3.3.

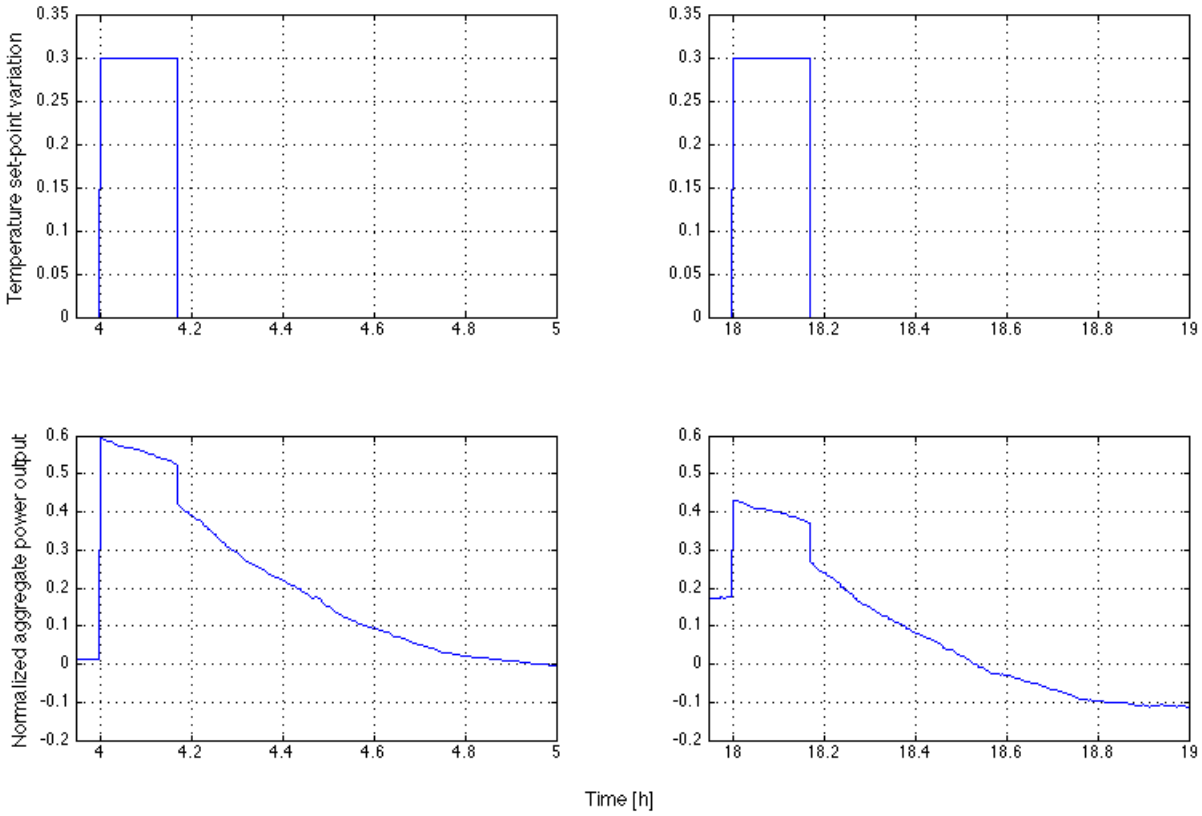

Figure 4.2: Counterexample for time invariance

4.3 ARMAX model structure

In this Section, we are looking for the plant of the aggregate EWH system, $G(z)$.
To achieve this, there are a variety of approaches:

1. **Markov models**: this is by far the most widely used model in the literature, as can be seen in the number of different groups working on this approach [2, 7, 8, 4].

   The main idea is to divide the temperature deadband δ into $\frac{N_{\text{bin}}}{2}$ temperature intervals, and assuming that each temperature interval can be again divided in TCLs ON and OFF switch state, which gives a total of N_{bin} state bins.

   Then, a state vector x is assembled, which contains the fraction of TCLs in each state bin out of the total number of TCLs. The state is often referred to as a vector of probability mass.

   To analytically derive the dynamics of such a model, a transition matrix A is assembled through Markov chains.

2. **PDE models**: Callaway [10], based on the mathematical work of Malhame and Chong [20], derived an elegant model description based on TCLs PDEs.

   Based on a statistical analysis of the aggregate system, and studying the influence of heterogeneity, Callaway arrived to an ARX and an ARMAX model descriptions. These describe an input-output relationship for the aggregate model.

   Note that in Callaway's case, the signals slightly differ from the ones defined in Section 4.1. Also, his application involves wind turbines, not EWHs.

3. **Input-Output models**: Perfumo et al. [1] proposed a second-order model that describes the system's aggregate dynamics based on first principles. This model is derived with methods of System Identification, and captures the aggregate power response for a population of ACs.

The approach used will be a combination between the 2. and 3. points: input-output data will be used to arrive to a time varying ARMAX model. The following derivations are based on Ljungs book [19].

The ARMAX model is an auto-regressive (AR) moving-average (MA) model, with exogenous input (X). The parameters of the model are obtained through solving a minimization problem.
Using the signals defined in Section 4.1, the input-output relationship can be defined as

$$A\left(z\right)\tilde{y}\left(k\right)=B_1\left(z\right)\hat{u}\left(k\right)+B_2\left(z\right)w^{\text{ave}}\left(k\right)+C\left(z\right)e\left(k\right), \tag{4.8}$$

where k is the discrete time variable, z is a complex number for the z-Transform, and $\tilde{y}$, $\hat{u}$ and w^{ave} are the known signals. Furthermore, e is the noise term, assumed to be Gaussian with $e\sim\mathcal{N}\left(0,\sigma_{\text{noise}}\right)$.
The polynomials are defined as follows: $A\left(z\right)\doteq 1+a_1z^{-1}+\ldots+a_nz^{-n}$, $B_1\left(z\right)\doteq b_1z^{-1}+\ldots+b_mz^{-m}$, $B_2\left(z\right)\doteq\bar{b}_1z^{-1}+\ldots+\bar{b}_{\bar{m}}z^{-\bar{m}}$ and $C\left(z\right)\doteq 1+c_1z^{-1}+\ldots+c_qz^{-q}$, with $\{n,\ m,\ \bar{m},\ q\}$ being the model orders.

In a next step, equation (4.8) is parametrized with the plant and noise sets $\{G\left(\theta,z\right)\}$ and $\{H\left(\theta,z\right)\}$:

$$\tilde{y}\left(k\right)=G\left(\theta,z\right)\cdot\begin{bmatrix}\hat{u}\left(k\right)\\ w^{\text{ave}}\left(k\right)\end{bmatrix}+H\left(\theta,z\right)\cdot e\left(k\right), \tag{4.9}$$

where $\theta\doteq\left[a_1,\ldots,a_n,b_1,\ldots,b_m,\bar{b}_1,\ldots,\bar{b}_{\bar{m}},c_1,\ldots,c_q\right]^T$ is the parameter vector, $G\left(\theta,z\right)\doteq\begin{bmatrix}\frac{B_1(z)}{A(z)} & \frac{B_2(z)}{A(z)}\end{bmatrix}$ and $H\left(\theta,z\right)\doteq\frac{C(z)}{A(z)}$.

The predictor for equation (4.9), denoted as $\hat{y}\left(k|\theta\right)$, is obtained as follows: with parameter vector θ and regressor vector at time k, $\varphi\left(k\right)$, the equation can be written as:

$$C\left(z\right)\hat{y}\left(k|\theta\right)=B_1\left(z\right)\hat{u}\left(k\right)+B_2\left(z\right)w^{\text{ave}}\left(k\right)+\left[C\left(z\right)-A\left(z\right)\right]\tilde{y}\left(k\right). \tag{4.10}$$

Using the definition for the prediction error $\epsilon\left(k,\theta\right)$, as well as the regressor vector $\varphi\left(k,\theta\right)$:

$$\begin{aligned}\epsilon(k,\theta) &\doteq \tilde{y}(k) - \hat{y}(k|\theta) \\ \varphi(k,\theta) &\doteq [-\tilde{y}(k-1),\ldots,-\tilde{y}(k-n),\hat{u}(k-1),\ldots,\hat{u}(k-m), \\ &\quad w^{\text{ave}}(k-1),\ldots,w^{\text{ave}}(k-\bar{m}),\epsilon(k-1,\theta),\ldots,\epsilon(k-p,\theta)]^T\end{aligned} \tag{4.11}$$

the equation (4.10) can be rewritten as

$$\hat{y}(k|\theta) = \varphi^T(k,\theta)\cdot\theta. \tag{4.12}$$

This is no linear regression, due to the nonlinear effect of θ in the regressor vector $\varphi(k,\theta)$. This kind of method is instead called *pseudolinear regression.*

To find the parameter vector solution $\hat{\theta}$, it is standard to define a minimization problem for the prediction error ϵ:

$$\begin{aligned}\hat{\theta} = \underset{\theta}{\text{argmin}} \quad & \|\epsilon\|_2 \\ \text{subject to} \quad & \epsilon = Y - \Phi\theta\end{aligned}, \tag{4.13}$$

with $Y \doteq [\tilde{y}(0),\ldots,\tilde{y}(N_{\text{sim}}-1)]^T$ and $\Phi \doteq \left[\varphi^T(0),\ldots,\varphi^T(N_{\text{sim}}-1)\right]^T$ and N_{sim} being the number of time steps to simulate.

4.4 Data setup and simulations

In this Section an ARMAX model will be derived using generated simulation data. The signals introduced in Section 4.1 will be the ones used here.
The simulation data will be partitioned into two different subsets: N_{exp} as the cardinality of the *experimental data*-set to generate the model and N_{val} as the cardinality of the *validation data*-set to validate the obtained model.

Selection of the signals

The applied external input $\hat{u}$ are pulses of duration $d \sim \text{Unif}(5,15)$ [min] (uniformly distributed, between 5 and 15 minutes).
The amplitudes used for these pulses are either positive or negative, denoted as $\hat{u}_+$ and $\hat{u}_-$ respectively, and there is an equal number of both of them. The intervals for these amplitudes are uniformly distributed with $\hat{u}_+ \sim \text{Unif}(U_+)$

and $\hat{u}_- \sim \text{Unif}(U_-)$. The limits U_+ and U_- will be selected as

$$\begin{array}{c} U_+ \doteq [0.25, 0.95] \\ U_- \doteq [-0.25, -0.95] \end{array} . \tag{4.14}$$

The set $\hat{u} \in]-0.25, 0.25[$ is avoided, because the signal level of the perturbation would be too small to be distinguished from the variances from the baseline (see Figure 3.4), especially for negative external inputs $\hat{u}_-$.

Therefore, the general formula for the inputs is:

$$\hat{u}(k) = \begin{cases} \hat{u}_{\{+,-\}} & , 60 \cdot h_{\text{start}} \text{ [min]} \leq \text{I}_i(k) \leq 60 \cdot h_{\text{start}} + d \text{ [min]} \\ 0 & , \text{I}_i(k) > 60 \cdot h_{\text{start}} + d \text{ [min]} \end{cases} , \tag{4.15}$$

where I_i is an hour long time interval, $\text{I}_{h_{\text{start}}} = [h_{\text{start}}, h_{\text{start}} + 1]$ [hour], h_{start} being the starting time of the pulse.

The external inputs were applied at different time intervals, starting at hours $h_{\text{start}} \in \{0, \ldots, 23\}$.
Consequently the output $\tilde{y}$ is defined as described in equation (4.2), and measured for the entire time interval $\text{I}_{h_{\text{start}}}$.

The last signal that will be used as an exogenous input is an averaged water draw w^{ave}, as defined in equation (4.3), with $N_E = 20$ experiments.

Model reformulation and properties

As was seen on Section 4.2, the simplified model is time varying and linear only for external inputs $\hat{u}$ of the same sign.
For this reason we are going to define the models

$$\overline{\mathcal{M}} \doteq \left\{ \mathcal{M}_0^+, \ldots, \mathcal{M}_{23}^+, \mathcal{M}_0^-, \ldots, \mathcal{M}_{23}^- \right\}, \tag{4.16}$$

where $\mathcal{M}_{h_{\text{start}}}^{\{+,-\}}$ is the ARMAX model for starting hour h_{start} and for external inputs with positive ($\hat{u}_+$) respectively negative ($\hat{u}_-$) sign.

The selection of the model orders $\{n,\ m,\ \bar{m},\ q\}$ is very important. They should remain as low as possible to avoid overestimation while being high enough to

capture the dynamics of the aggregate population $\mathcal{P}$. A lower set of model orders will also be beneficial in terms of computational time when applying the controller in Chapter 5.
The selected model orders are

$$\{n,\ m,\ \bar{m},\ q\} = \{4,\ 4,\ 4,\ 1\}\,. \tag{4.17}$$

The model order was selected as 4 because there was no benefit for higher orders (5 or above), since the fit from Table 4.1 did not improve when increasing this order. The choice for order q was more complicated, as there were similar performing ones, so the final choice was taken also keeping in mind that the model order should remain as low as possible. In the end, higher values for q were not selected because the fit remained almost identical as in Table 4.1, only adding complexity to the model.
It is important to note that the selected model orders should remain equal for all models in (4.16). What should be changing when a new hour enters is the parameter vector θ, but not the model structure $\mathcal{M}$ itself. This allows for repurpose of the model structure $\mathcal{M}$ in the controller design of Chapter 5.

The ARMAX model $\mathcal{M}_{h_{\text{start}}}^{\{+,-\}}$ can be reformulated into a state-space model $\mathcal{S}_{h_{\text{start}}}^{\{+,-\}}$ for starting hour h_{start}. These models have the form:

$$\begin{array}{rcl} x\left(k+1\right) & = & Ax\left(k\right) + B_1\hat{u}\left(k\right) + B_2 w^{\text{ave}}\left(k\right) + Ke\left(k\right) \\ \tilde{y}\left(k\right) & = & Cx\left(k\right) + D_1\hat{u}\left(k\right) + D_2 w^{\text{ave}}\left(k\right) + e\left(k\right) \end{array}\,, \tag{4.18}$$

where $x \in \mathcal{X} \subseteq \mathbb{R}^{n,1}$ is the state vector, K is the state disturbance matrix and $\{A, B_1, B_2, C, D_1, D_2\}$ are the state-space matrices.
Important to note is that the initial state $x\left(0\right)$ will not be estimated. Instead, it is assumed to be zero: $x\left(0\right) = 0^{n,1}$.

Of course, the models $\overline{\mathcal{M}}$ should also be asymptotically stable, controllable and observable.
All the models displayed on Table 4.1 maintain these properties, and are asymp-

totically stable[1], controllable [2] and observable [3].

Identified models

The N_{exp} experimental data simulations are used to generate the ARMAX models $\overline{\mathcal{M}}$, calculating the parameter vector θ as described in Section (4.3).
The N_{val} validation data simulations are used to assess the validity of the obtained linear ARMAX models, and compare the responses generated through the models $\overline{\mathcal{M}}$ against the real response from the system that is being modelled. The fit is calculated with the NRSME definition:

$$\text{fit} \doteq 100 \cdot \left(1 - \frac{\|\tilde{y} - y_{\text{ARMAX}}\|}{\|\tilde{y} - \text{mean}\,(\tilde{y})\|}\right) [\%]\,, \tag{4.19}$$

where $\tilde{y}$ is the validation data output signal and y_{ARMAX} is the output signal generated from the ARMAX model.

Table 4.1 summarizes some resuls for the fit equation (4.19) for different starting hours $h_{\text{start}} \in \{4, 7, 12, 16, 18, 20, 22\}$.
There were $N_{\text{exp}} = 70$ experimental and $N_{\text{val}} = 70$ validation data signals for each hour and for each sign of the external input $\hat{u}_+$, $\hat{u}_-$.

As can be seen in the Table's values, for $\hat{u}_+$ the average fit for most hours is well above 70 percent, with small standard deviation.
On the other hand, for $\hat{u}_-$ the fits are much lower, but the relatively small set N_{ON} for the baseline, as discussed in Section (3.3), makes that for negative values the fit is worse.
Hour 4 presents a worse fit, but it is to be expected due to the small signal level of the baseline. At the first hours of the day the set N_{ON} is so small (see Figure 3.4), that changes around the baseline (especially for $\hat{u}_-$) will be have a low signal-to-noise ratio.

[1] A discrete-time model $\mathcal{S}_{h_{\text{start}}}^{\{+,-\}}$ is asymptotically stable if and only if $\lambda_i\,(A) < 1\ \forall i = 1, \ldots, n$.

[2] A discrete-time model $\mathcal{S}_{h_{\text{start}}}^{\{+,-\}}$ is controllable if and only if the matrix $\left[B_1\ AB_1\ A^2B_1\ \ldots\ A^{n-1}B_1\right] \in \mathbb{R}^{n,n\cdot m}$ has full rank.

[3] A discrete-time model $\mathcal{S}_{h_{\text{start}}}^{\{+,-\}}$ is observable if and only if the matrix $\left[C\ CA\ CA^2\ \ldots\ CA^{n-1}\right]^T \in \mathbb{R}^{n\cdot p,n}$ has full rank.

$h_{\mathbf{start}}$	$\hat{u}_+$		$\hat{u}_-$	
	μ fit [%]	σ fit [%]	μ fit [%]	σ fit [%]
4	64.4381	19.7403	26.203	23.8297
7	68.4144	11.238	55.9121	19.4455
12	75.1791	10.1283	60.8689	15.5004
16	74.7440	10.1256	52.4389	22.5337
18	74.1694	9.2298	56.9006	20.6073
20	77.6904	8.1194	60.7367	19.1827
22	73.1659	10.2441	49.4251	27.5658

Table 4.1: Fit of the models $\mathcal{M}_{h_{\text{start}}}^{\{+,-\}}$ to the validation data

Selected examples

The following examples show some of the results of Table 4.1.
Figure 4.3 represents four different examples, one for each of the models $\mathcal{M}_{20}^{+}$, $\mathcal{M}_{12}^{-}$, $\mathcal{M}_{18}^{+}$ and $\mathcal{M}_{16}^{-}$. The fit percentage (from equation 4.19) is at the top of each subplot.
The upper row of subplots shows examples where the models capture the dynamics of the system well, whereas the lower subplots are examples where the fit is worse (for example by overshooting in the low-right subplot).

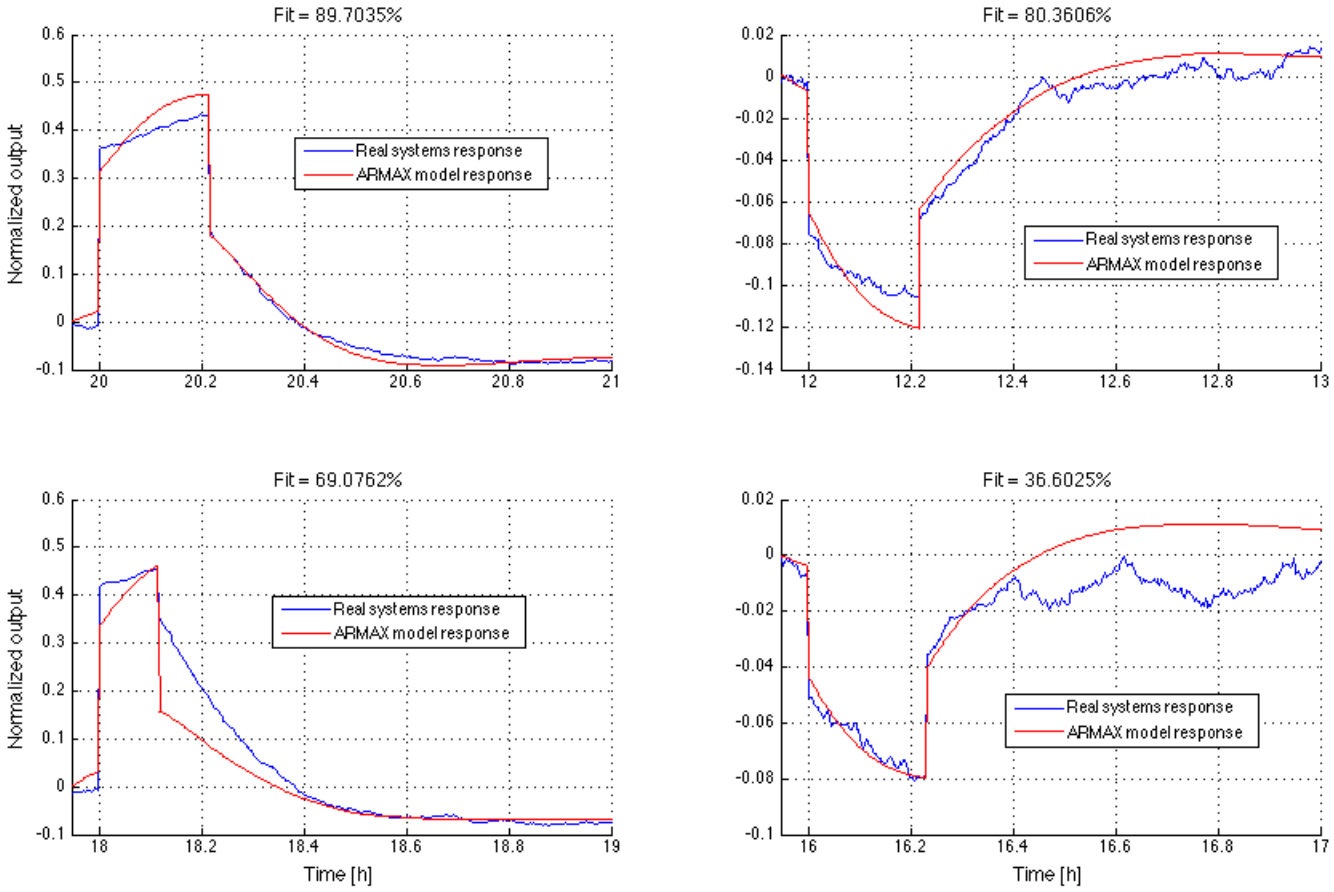

Figure 4.3: Selected examples for ARMAX models

Chapter 5

Optimization problem

This Chapter will define an optimization problem for the EWH population system. It will furthermore be reformulated into a finite-horizon Sequential Convex Quadratic Program (SCQP), whose solution will give a control sequence of lenght N, $U_{0\to N} = \{\hat{u}(0), \hat{u}(1), \ldots, \hat{u}(N-1)\}$.
This will act as the controller for the system, as the computed optimal input trajectory $U^*_{0\to N}$ will be applied to the aggregate population $\mathcal{P}$, and the resulting aggregate power trajectory compared to a reference signal.
Indeed, the choices for a controller structure are plenty for a linear model, as assumed in the model derived in Chapter 4. What motivated the SCQP were the convexity property, which ensures the existence of a minimizer of the cost function, the number of available computational optimization solvers (`Gurobi` [21] was the one used here), and having time-domain data.

As for the organization, Section 5.1 deals with general optimization definitions, 5.2 explains the reformulation into a SCQP problem, and lastly 5.3 shows some simulation results of the implementation of the problem.

5.1 Optimization concepts

In optimization, the goal is to minimize an objective function J,

$$J_{0\to N}(x_0, U_{0\to N}) \doteq p(x_N) + \sum_{k=0}^{N-1} q(x(k), \hat{u}(k)), \tag{5.1}$$

given some initial condition $x_0 \doteq x(0)$ over a time horizon N. In the above definition, $p : \mathcal{X}_\mathrm{f} \to \mathbb{R}$ is the final cost, and $q : \mathcal{X} \times \mathcal{U} \to \mathbb{R}$ is the stage cost. Note that the final state $x(N)$ should remain within the set $\mathcal{X}_f$: $x(N) \in \mathcal{X}_f$.

We are faced with a finite horizon problem. This means that only N time steps $k = \{0, \ldots, N-1\}$ will be evaluated at every solution of the optimization problem, but only the computed input will be stored. This is the receding horizon strategy used in MPC controllers.

In this discrete-time optimal control problem the minimization is achieved by calculating the optimal input sequence $U^*_{0\to N} = \{\hat{u}^*(0), \hat{u}^*(1), \ldots, \hat{u}^*(N-1)\}$ over the finite-time horizon N. This input sequence is then applied to the dynamical system. This yields the optimal cost sequence $J^*_{0\to N}$,

$$J^*_{0\to N}(x_0) \doteq \min_{U_{0\to N}} J_{0\to N}(x_0, U_{0\to N}). \tag{5.2}$$

Some examples for appropiate convex objective functions J are listed in the following table:

Index	What to penalize	Formula for the cost J
1	The output tracking error	$p(x_N) + \sum_{k=0}^{N-1} \left\|\tilde{y}(k) - P^{\mathrm{ref}}(k)\right\|_2^2$
2	The control input vector	$p(x_N) + \sum_{k=0}^{N-1} \|\hat{u}(k)\|_2^2$
3	Changes between consecutive inputs	$p(x_N) + \sum_{k=0}^{N-2} \|\hat{u}(k+1) - \hat{u}(k)\|_2^2$
4	Inputs far from the boundary	$p(x_N) + \sum_{k=0}^{N-1} \|\hat{u}(k) - \hat{u}_{\max}\|_2^2$

Table 5.1: Possible penalizations for the cost function (5.1)

The most important penalization is number 1, where the objective is to track the reference signal for the aggregate power, P^{ref}.
Also to note is that the stage cost of objective number 3 can only go up to $N-2$ to avoid using unavailable inputs. Objective number 4 is the opposite from number 2, and assumes that $\hat{u}_{\min} = -\hat{u}_{\max}$.

For the remainder of this Chapter, objective 1 will be the one used as the objective function (5.1).

An additional requirement for defining the optimization problem are the constraints. Note that in this problem only *linear* constraints will be considered (linear in the optimization variable). They can be categorized into *equality* and *inequality* constraints:

$$\begin{aligned} A_{\text{eq}} \cdot z &= b_{\text{eq}} \\ A_{\text{ineq}} \cdot z &\leq b_{\text{ineq}} \end{aligned} , \tag{5.3}$$

where A_{eq} is the equality matrix, b_{eq} denotes the equality vector, A_{ineq} is the inequality matrix, b_{ineq} the inequality vector, and z is the optimization variable. Taking into account the state-space model dynamics $\mathcal{S}$ of equation (4.18) in Section 4.3, the dynamics of the system for computing $x(k+1)$ will be appearing as the equality constraints in the optimization problem at hand.

Lastly, the optimization variable $z \in \mathcal{Z}$ can also be bounded. For our problem, the only contrained variable is the external input $\hat{u}$. As was described in Section 4.1, the temperature set-point variation $\hat{u} \in \mathcal{U}$, and the space $\mathcal{U} \subseteq [-1, 1]$, are given in relative terms. In 4.1 that set was tightened, however a compact convex set should be maintained later on.
Denoting lb as the lower bound and ub as the upper bound, the general definition for the boundaries can be written as

$$lb \leq z \leq ub. \tag{5.4}$$

Summary

The optimization problem for the controller can be summarized as follows:

$$\begin{aligned} \min_{u} \quad & p(x_N) + \sum_{k=0}^{N-1} \left\| \tilde{y}(k) - P^{\text{ref}}(k) \right\|_2^2 \\ \text{s.t.} \quad & x(k+1) = Ax(k) + B_1 \hat{u}(k) + B_2 w^{\text{ave}}(k) + Ke(k) \\ & \tilde{y}(k) = Cx(k) + D_1 \hat{u}(k) + D_2 w^{\text{ave}}(k) + e(k) \\ & -\hat{u}_{\min} \leq \hat{u}(k) \leq \hat{u}_{\max}, \ \forall k \in \{0, \ldots, N-1\} \end{aligned} , \tag{5.5}$$

which should be adapted into the Quadratic Program (QP) form in the next Section (5.2), with quadratic cost and linear constraint functions.

5.2 Sequential Convex Quadratic Program formulation

In this Section the optimization problem of equation (5.5) will be transformed into a Sequential Convex Quadratic Program (SCQP).

Quadratic Program and state augmentation

A Quadratic Program has quadratic cost and linear constraint functions with respect to the optimization variable. In addition the feasible set is a polyhedron. Convexity is granted if the quadratic matrix Q is positive semi-definite ($Q \succeq 0$). The CQP problem can be written as

$$\begin{array}{ll} \min\limits_{z} & \frac{1}{2} z^T Q z + R^T z + \alpha \\ \text{s.t.} & A_{\text{eq}} \cdot z = b_{\text{eq}} \\ & A_{\text{in}} \cdot z \leq b_{\text{in}} \\ & lb \leq z \leq ub \end{array} , \tag{5.6}$$

where Q is the matrix for the quadratic cost, R is the vector for linear cost, α is the affine term, A_{eq} is the matrix for the equality constraints, b_{eq} is the vector for the equality constraints, A_{in} is the matrix for the inequality constraints, b_{in} is the vector for the inequality constraints, lb and ub are the lower - and upper boundaries and z is the optimization variable.

The optimization variable z is time dependant, and defined as $z(k) \doteq [x(k), \hat{u}(k)]^T$. When transforming the tracking cost function from equation (5.5) into the notation of (5.6), the matrices have the following structures:

$$\begin{aligned} Q_k &= \begin{bmatrix} C^T C & C^T D_1 \\ D_1^T C & D_1^T D_1 \end{bmatrix} \\ R_k^T &= \begin{bmatrix} \left(-P^{\text{ref}}(k) + D_2 w^{\text{ave}}(k)\right) \cdot 2C \\ \left(-P^{\text{ref}}(k) + D_2 w^{\text{ave}}(k)\right) \cdot 2D_2 \end{bmatrix} \\ \alpha_k &= \left(D_2 w^{\text{ave}}(k)\right)^2 - 2 D_2 w^{\text{ave}}(k) + \left(P^{\text{ref}}(k)\right)^2 \end{aligned} . \tag{5.7}$$

Note that time dependency was added for the matrices and the optimization variable z_k (however notice that $Q_k = Q \; \forall k$).
The terminal cost matrix P_{T} is constructed to keep convexity, and selected with the form $P_{\text{T}} = \text{diag}(p_{\text{T}}, \ldots, p_{\text{T}})$, $p_{\text{T}} \geq 0$.

Time rollout for Sequential part

Now the unfolding of the time horizon N into the time instances $\{0, \dots, N-1\}$ will follow.
This is a standard procedure in MP Controllers (MPCs). At each time step the calculations for an entire horizon are computed, but only the first control action is finally implemented.

The roll-out state $\tilde{z}$ can be defined as

$$\tilde{z} \doteq [z(0), z(1), \dots, z(N-1), z(N)], \tag{5.8}$$

with $z(k)$ being the augmented state at time k. Note that contrary to previous time steps, where $z(k) \doteq [x(k), \hat{u}(k)]^T$, the final time instance is defined as: $z(N) \doteq x(N)$.

Now optimization quadratic and linear matrices can be defined as

$$\begin{aligned} \tilde{Q} &\doteq \begin{bmatrix} Q & & & 0 \\ & \ddots & & \\ & & Q & \\ 0 & & & P \end{bmatrix}, \\ \tilde{R} &\doteq \begin{bmatrix} R_0^T & R_1^T & \cdots & R_{N-1}^T & 0^T \end{bmatrix} \end{aligned} \tag{5.9}$$

as the elements of Q_k do not depend on time, with $\tilde{Q}$ as the quadratic block-diagonal unfolded matrix and $\tilde{R}$ as the linear unfolded matrix.

Evaluating the state space dynamics $\mathcal{S}$ of equation (4.18) at the time values $k = \{0, \dots N\}$, and formulating it for the augmented state z, the structure

$$\begin{aligned} \begin{bmatrix} \mathbb{I}_n & 0 \end{bmatrix} z(0) &= x_0 \\ \begin{bmatrix} A & B_1 \end{bmatrix} z(0) + \begin{bmatrix} -\mathbb{I}_n & 0 \end{bmatrix} z(1) &= -B_2 w^{\text{ave}}(0) \\ \begin{bmatrix} A & B_1 \end{bmatrix} z(1) + \begin{bmatrix} -\mathbb{I}_n & 0 \end{bmatrix} z(2) &= -B_2 w^{\text{ave}}(1) \\ &\vdots \\ \begin{bmatrix} A & B_1 \end{bmatrix} z(N-1) + \begin{bmatrix} -\mathbb{I}_n \end{bmatrix} z(N) &= -B_2 w^{\text{ave}}(N-1) \end{aligned} \tag{5.10}$$

follows, and using the roll-out state $\tilde{z}$ (5.8), the equality constraints are found:

$$A_{\text{eq}} = \begin{bmatrix} \begin{bmatrix} \mathbb{I}_n & 0 \\ A & B_1 \end{bmatrix} & & & & \\ & \begin{bmatrix} -\mathbb{I}_n & 0 \\ A & B_1 \end{bmatrix} & & & \\ & & \begin{bmatrix} -\mathbb{I}_n & 0 \end{bmatrix} & & \\ & & & \ddots & \ddots \\ & & & \begin{bmatrix} A & B_1 \end{bmatrix} & \begin{bmatrix} -\mathbb{I}_n \end{bmatrix} \end{bmatrix}$$
$$b_{\text{eq}} = \begin{bmatrix} x_0 & -B_2 w^{\text{ave}}(0) & -B_2 w^{\text{ave}}(1) & \dots & -B_2 w^{\text{ave}}(N-1) \end{bmatrix}^T . \tag{5.11}$$

Lastly, to reformulate the boundaries into the unfolded augmented state $\tilde{z}$, the boundary vectors lb and ub are defined as

$$\begin{aligned} lb &= \begin{bmatrix} -\infty_n & \hat{u}_{\min} & -\infty_n & \hat{u}_{\min} & \dots & -\infty_n & \hat{u}_{\min} & -\infty_n \end{bmatrix}^T \\ ub &= \begin{bmatrix} \infty_n & \hat{u}_{\max} & \infty_n & \hat{u}_{\max} & \dots & \infty_n & \hat{u}_{\max} & \infty_n \end{bmatrix}^T \end{aligned} . \tag{5.12}$$

No constraints are formulated for the state x because it was artificially introduced by the model structure transformation (from ARMAX $\mathcal{M}$ to state-space $\mathcal{S}$).

The constraints for the external input $\hat{u}$, $\hat{u}_{\min}$ and $\hat{u}_{\max}$, are given by the construction of the input space $\mathcal{U}$. This selection was discussed in Section 4.1, however it should be noted that the set $\mathcal{U}$ should be convex.

Summary

The reformulation yields a SCQP optimization problem of the form

$$\begin{aligned} \min_{\tilde{z}} \quad & \tilde{z}^T \tilde{Q} \tilde{z} + \tilde{R}^T \tilde{z} + \sum_{k=0}^{N-1} \alpha_k \\ \text{s.t.} \quad & A_{eq} \cdot \tilde{z} = b_{eq} \\ & lb \leq \tilde{z} \leq ub \end{aligned} , \tag{5.13}$$

which computes the optimal control trajectory $U^*_{t \to t+N} \doteq \{\hat{u}^*(t), \hat{u}^*(t+1), \dots, \hat{u}^*(t+N-1)\}$ for every simulation time step t.

5.3 Selected simulation results

In this Section, some simulation examples for the controller will be displayed. The model selected is the state-space model $\mathcal{S}_{h_{\text{start}}}^{\{+,-\}}$ with starting hour h_{start}, as presented in equation (4.18). Note that the noise signal e is discarded, as already seen when deriving the equality constraints (5.10).
The remaining selected values and setup for the optimization controller are listed below:

- The time horizon is $N = 30$, and the simulated steps are $N_{\text{sim}} = 360$.
- The terminal cost is selected as $p = 10$.
- The boundaries for equation (5.12) are varied, and either $[\hat{u}_{\min}, \hat{u}_{\max}] \doteq [0, 0.95]$ or $[\hat{u}_{\min}, \hat{u}_{\max}] \doteq [-0.95, 0.95]$.

On all the following figures, the upper subplot shows the optimal input trajectory $U^*_{0\to N}$, computed by the controller. The lower subplot shows three different signals: the reference signal P^{ref} (in black), the trajectory $U^*_{0\to N}$ applied to the state-space model $\mathcal{S}_{h_{\text{start}}}^{\{+,-\}}$ (in red) and the trajectory $U^*_{0\to N}$ applied to the real system (in blue).

Figure 5.1 shows the tracking of a trapezoidal positive reference signal. The model used was $\mathcal{S}_{16}^{+}$. As can be seen, in this case the tracking performance is quite good, for both the red and blue lines. Note that the boundaries are $[\hat{u}_{\min}, \hat{u}_{\max}] \doteq [0, 0.95]$ in this case. On Figure 5.2 the same reference signal is tracked, but this time with relaxed boundaries, $[\hat{u}_{\min}, \hat{u}_{\max}] \doteq [-0.95, 0.95]$.

The second example, Figures 5.3 and 5.4 show an input with complete different form compared to the pulse inputs used to generate the models (equation (4.15)). In this case, the first model used is $\mathcal{S}_{16}^{+}$, at $h_{\text{start}} = 16$, and the second model used is $\mathcal{S}_{20}^{+}$, at $h_{\text{start}} = 20$. This example aims to show the differences in performance when selecting the hour when the reference signal is applied. It is clear that 5.4 has a much lower performance than 5.3.

Figures 5.5 and 5.6 show a a refenrence input close to the pulses used to create the ARMAX models, but with a "bump". As can be seen, the controller can not react to this one oscillation well, despite following the general shape of the pulse well. This is probably due to the small duration of the "bump". When constructing the models in Chapter 4, the pulse durations for the inputs were uniformly distributed between 5 and 15 minutes.

Lastly, the examples 5.7 and 5.8 show an interesting example with the reference signal being two positive sinusoidal oscillations. As can be seen, the controller follows the first oscillation well. However, the second oscillation performs poorly. After the first oscillation, some EWHs switched to the ON state, thus warming the interior of the tank. As the oscillations are of high duration, and the oscillations are consecutive, the system is not prepared for the second power increase. The system has no time to recover to the baseline level where the models where identified from.

All in all, the controller has good performance for reference signals that follow a similar pattern to the one used to identify the system. The controller is tracking the trajectories perfectly, as can be seen if observing the red line of the figures. The main challenge lays still in model design, as the mismatch between the ARMAX - and state-space models and the real system is still quite high.

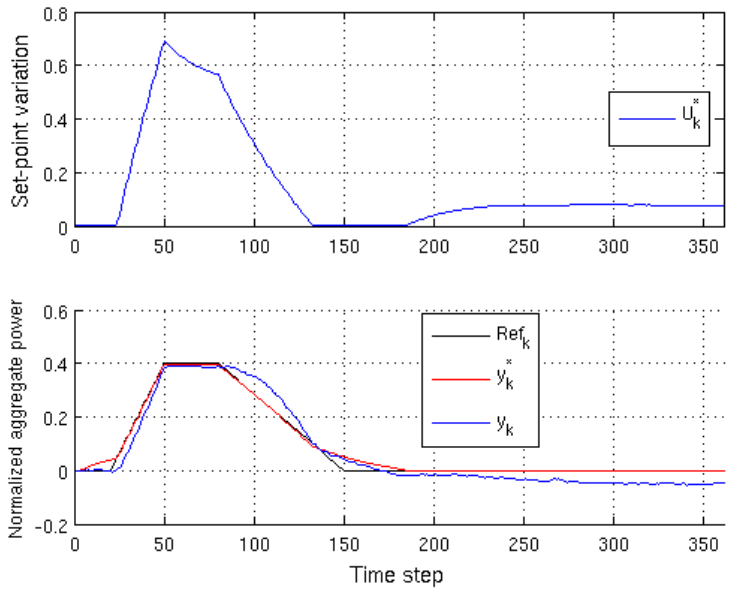

Figure 5.1: $\mathcal{S}_{16}^{+}$ with $[\hat{u}_{\min}, \hat{u}_{\max}] \doteq [0, 0.95]$

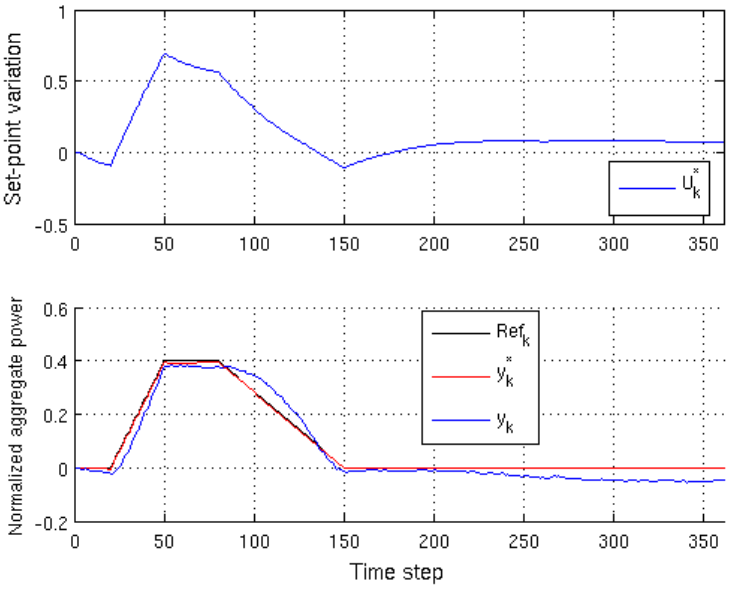

Figure 5.2: $\mathcal{S}_{16}^{+}$ with $[\hat{u}_{\min}, \hat{u}_{\max}] \doteq [-0.95, 0.95]$

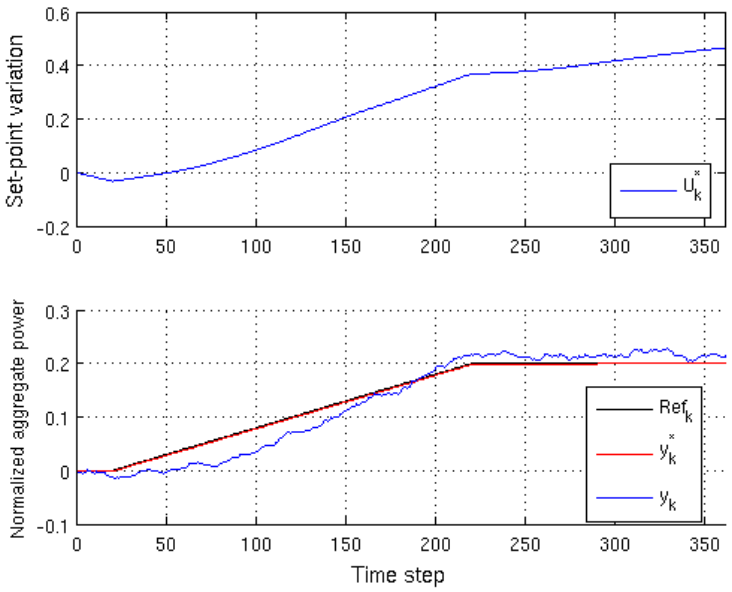

Figure 5.3: $\mathcal{S}_{16}^{+}$ with $[\hat{u}_{\min}, \hat{u}_{\max}] \doteq [-0.95, 0.95]$

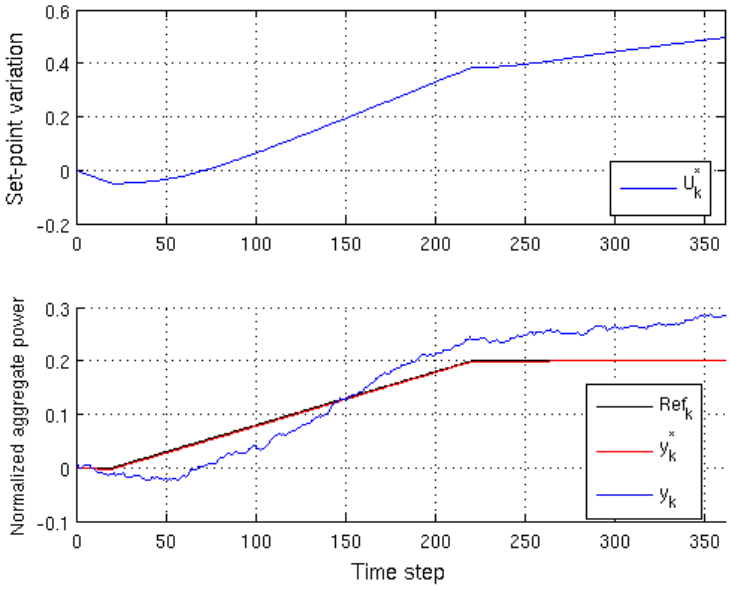

Figure 5.4: $\mathcal{S}_{20}^{+}$ with $[\hat{u}_{\min}, \hat{u}_{\max}] \doteq [-0.95, 0.95]$

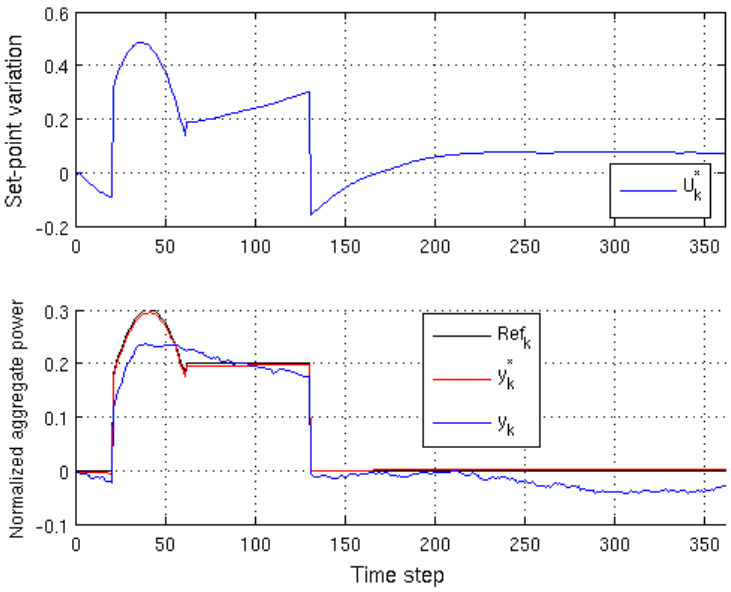

Figure 5.5: $\mathcal{S}_{16}^{+}$ with $[\hat{u}_{\min}, \hat{u}_{\max}] \doteq [-0.95, 0.95]$

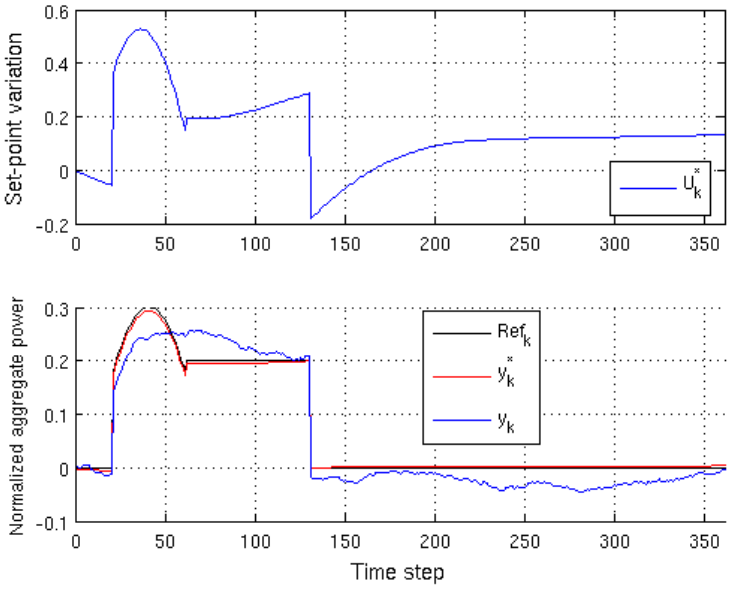

Figure 5.6: $\mathcal{S}_{20}^{+}$ with $[\hat{u}_{\min}, \hat{u}_{\max}] \doteq [-0.95, 0.95]$

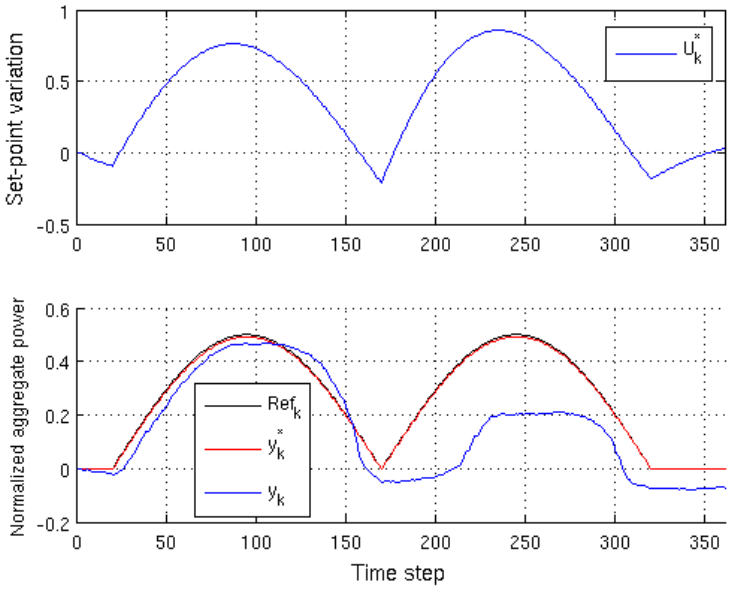

Figure 5.7: $\mathcal{S}_{16}^{+}$ with $[\hat{u}_{\min}, \hat{u}_{\max}] \doteq [-0.95, 0.95]$

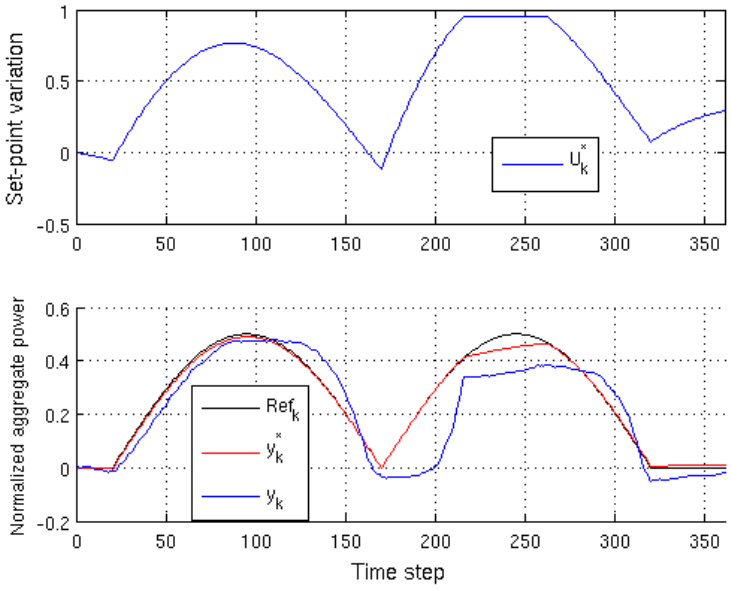

Figure 5.8: $\mathcal{S}_{20}^{+}$ with $[\hat{u}_{\min}, \hat{u}_{\max}] \doteq [-0.95, 0.95]$

Chapter 6

Conclusion

This project presented the derivaton of an aggregated model for a population of EWHs, which with the use of a controller was able to track given reference power trajectory. For this, the individual EWH model by Vrettos et al. [6] was used.

Then, system properties for an aggregated population of loads were studied. The baseline power consumption of the population was characterized for different number of loads N_{app}. As a conclusion, a trade-off had to be found between the number of loads, which reduced the variance from the nominal baseline, and computational time.

Also of special importance were the linearity and time invariance properties. It turns out that the system is time varying, and linearity can only be assumed throughout certain hours of the day, when the baseline levels are high enough (after 10 am, see Figure 3.4), and the RMSE is therefore low enough.

The signals used for the aggregate model were defined, and the model structure derived using System Identification techniques. The fit to validation data of these models was found to be better at hours where the linearity property was assumed.

At last, the MPC controller was designed for reference signal tracking in the aggregate power. This controller performed well to the examples tested, with good tracking performance for signals similar to the ones used for identification. It was noted that for consecutive controller disturbances from the baseline, some recovering time between them should be maintained. If not, the system will be at a different state from that of the identified model for that hour, thus performing badly (see Figures 5.7 and 5.8) for the second disturbance. In

summary, the controller has good performance for reference signals that follow a similar pattern to the one used to identify the system. This MPC controller is also quite efficient as the solving could be implemented in real-time efficiently with the existing sampling interval of the system.
However, the main challenge lays still in model design, as the mismatch between the models and the real system is still quite high in some cases. Also, the optimization problem became infeasible for horizons twice as big as the one selected, which should not necessarily pose a problem, but it should be addressed.

6.1 Outlook

There are a variety of interesting challenges to be studied in the future, as for example:

- The identified models are still not good enough in terms of fit to the real system. This should be improved gaining more system insight, redefining the selected signals if necessary, and using more experimental and validation points. As the deviations from the baseline are being used for the output, the averaged water draw signal w^{ave} did have a very small impact in the model, therefore it should be studied or redefined.

- Also, a quantitative comparison between these ARMAX models and the more preferred Markov-chain models should be performed. Concepts like the state of charge, which is a normalized signal giving more information than the mere switch state, are already under use and of high interest. The work by Koch et al. [8] defines such a bin model, and also uses a MPC, so this would be a good project to compare with.

- Lastly, a study about the EWH thermostat sensors would be very beneficial. Callaway [10] did a comparison of sensor resolution versus RMSE performance for another type of device. Such a comparison would be insightful. Also, the communication protocols and capabilities of these sensors should be addressed. These is of extreme importance when studying the implementation of the algorithms into EWHs and deployment of controllers into real systems. This is being addressed in the literutre, as for example in [**?**].

Bibliography

[1] C. Perfumo, E. Kofman, J. H. Braslavsky, and J. K. Ward, "Load management : model-based control of aggregate power for populations of thermostatically controlled loads," 2000.

[2] S. Bashash and H. K. Fathy, "Modeling and Control of Aggregate Air Conditioning Loads for Robust Renewable Power Management," vol. 21, no. 4, pp. 1318–1327, 2013.

[3] K. Kalsi, M. Elizondo, J. Fuller, S. Lu, and D. Chassin, "Development and Validation of Aggregated Models for Thermostatic Controlled Loads with Demand Response," *2012 45th Hawaii International Conference on System Sciences*, pp. 1959–1966, Jan. 2012.

[4] W. Zhang, J. Lian, C.-y. Chang, and S. Member, "Aggregated Modeling and Control of Air Conditioning Loads for Demand Response," vol. 28, no. 4, pp. 4655–4664, 2013.

[5] J. Kondoh, N. Lu, S. Member, and D. J. Hammerstrom, "An Evaluation of the Water Heater Load Potential for Providing Regulation Service," 2011.

[6] E. Vrettos, S. Koch, and G. Andersson, "Load frequency control by aggregations of thermally stratified electric water heaters," *IEEE PES Innovative Smart Grid Technologies Conference Europe*, pp. 1–8, 2012.

[7] S. Kundu, N. Sinitsyn, S. Backhaus, and I. Hiskens, "Modeling and control of thermostatically controlled loads," Jan. 2011.

[8] S. Koch, J. L. Mathieu, and D. S. Callaway, "Modeling and Control of Aggregated Heterogeneous Thermostatically Controlled Loads for Ancillary Services," 2011.

[9] A. C. Kizilkale and R. P. Malhame, "Collective Target Tracking Mean Field Control for Markovian Jump-Driven Models of Electric Water Heating Loads," pp. 1867–1872, 2014.

[10] D. S. Callaway, "Tapping the energy storage potential in electric loads to deliver load following and regulation, with application to wind energy," *Energy Conversion and Management*, vol. 50, pp. 1389–1400, May 2009.

[11] L. C. Totu, J. Leth, and R. Wisniewski, "Control for large scale demand response of thermostatic loads *," 2013.

[12] J. L. Mathieu and D. S. Callaway, "State estimation and control of heterogeneous thermostatically controlled loads for load following," *Proceedings of the Annual Hawaii International Conference on System Sciences*, pp. 2002–2011, 2011.

[13] L. C. Totu and R. Wisniewski, "Demand Response of Thermostatic Loads by Optimized Switching-Fraction Broadcast," 2014.

[14] S. Koch, "Demand Response Methods for Ancillary Services and Renewable Energy Integration in Electric Power Systems," no. 20470, 2012.

[15] I. Dincer and M. a. Rosen, "Thermal energy storage systems and applications, second edition," 2011.

[16] A. Mathematics, S. Journal, and N. Analysis, "Stability Restrictions on Second Order , Three Level Finite Difference Schemes for Parabolic Equations Author (s): J . M . Varah Source : SIAM Journal on Numerical Analysis , Vol . 17 , No . 2 (Apr ., 1980), pp . 300-309 Published by : Society for Ind," vol. 17, no. 2, pp. 300–309, 2011.

[17] J. Lutz, "Water Heaters And Hot Water Distribution Systems," 2012.

[18] W. Healy, J. Lutz, and A. Lekov, "Variability in Energy Factor Test Results for Residential Electric Water Heaters," *HVAC&R Research*, vol. 9, no. February 2015, pp. 435–449, 2003.

[19] L. Ljung, *System Identification: theory for the user*. 1999.

[20] R. Malhame and Chee-Yee Chong, "Electric load model synthesis by diffusion approximation of a high-order hybrid-state stochastic system," *IEEE Transactions on Automatic Control*, vol. 30, no. 9, pp. 854–860, 1985.

[21] "Gurobi optimization solver." http://www.gurobi.com. Last accessed: 03.04.2015.

Appendix A

Linearity examples

Example 1

To assess the linearity property of the system, as described in Section 4.2, the following examples will be studied.
In this experiment the input space will be sampled to assess if $\tilde{y}(\hat{u}_1 + \hat{u}_2) = \tilde{y}(\hat{u}_1) + \tilde{y}(\hat{u}_2)$, $\hat{u}_1, \hat{u}_2 \in \mathcal{U}$. This will check the additivity property of the system.
In addition, the following assumptions are made regarding the setup:

- The starting hours used for the simulation interval $\mathrm{I}_{h_{\text{start}}} \doteq [h_{\text{start}}, h_{\text{start}} + 1]$ [hour] are $h_{\text{start}} = \{4, 7, 12, 20\}$.
- The input has the form of equation (4.15) with duration $d = 10$ [min].
- The input space was sampled, with $\hat{u}_1 > 0, \hat{u}_2 > 0$, with
  - 100 samples $\hat{u}_1, \hat{u}_2 \sim \text{Unif}(0.2, 0.45)$ and
  - 30 samples with $\hat{u}_1 \sim \text{Unif}(0.5, 0.75)$ and $\hat{u}_2 \sim \text{Unif}(0.1, 0.2)$.
    This is to address the case where an input is much higher than the other ($\hat{u}_1 \gg \hat{u}_2$).

Figures A.1 and A.2 show the simulation results for **Example 1**. For both the RMSE between $\tilde{y}(\hat{u}_1 + \hat{u}_2)$ and $\tilde{y}(\hat{u}_1) + \tilde{y}(\hat{u}_2)$ is computed.
In Figure A.1 , the number of simulation experiments that fall into a RMSE [%] bin are displayed. As can be seen, hours $4, 7$ have a much higher RMSE than hours $12, 20$. Figure A.2 shows the RMSE on the y-axis and the value of $\hat{u}_1 + \hat{u}_2$ on the x-axis. As can be seen the RMSE increases, as the sum increases, and

the data-points where $\hat{u}_1 \gg \hat{u}_2$ have a smaller error (for the same hour) than the other 100 sampled input pairs. Note that the RMSE remains below 12 [%] in all samples.

Example 2

The second example addresses the case where both inputs are of same magnitude but different sign: $\hat{u}_1 + \hat{u}_2 = 0$, with $\hat{u}_1 \doteq -\hat{u}_2,\ \hat{u}_1, \hat{u}_2 \in \mathcal{U}$.
In this case $\tilde{y}\,(\hat{u}_1 + \hat{u}_2)$ near zero would be the expected result.
The sampling will be the following:

- The starting hours used for the simulation interval $\mathrm{I}_{h_{\text{start}}} \doteq [h_{\text{start}}, h_{\text{start}} + 1]$ [hour] are $h_{\text{start}} = \{4, 7, 12, 20\}$.
- The input has the form of equation (4.15) with duration $d = 10$ [min].
- A total of 20 input samples were used per hour, with $\hat{u}_1 \sim \text{Unif}\,(0.2, 0.6)\,, \hat{u}_2 = -\hat{u}_1$.

Figure A.3 shows the histogram for the simulation results. The RMSE for hours $4, 7$ is much higher than that of hours $12, 20$. This was to expect, since due to the baseline only a maximum of about 25 [%] for the set N_{ON} at any given time of the day (see Figure 3.4). The evolution of the baseline points towards this behaviour.
For example at hour $h_{\text{start}} = 7$, applying $\hat{u}_2 = -0.5$ achieves a much lower signal level than at hour $h_{\text{start}} = 20$, simply because the set N_{ON} is at the 10 [%] range as compare to the 20 [%] range of the latter.
These results are consistent with the ones observed in **Example 1**.

In summary, the linearity property should be considered only in cases where the signal level is high enough, and when both inputs have the same sign. In hours where the baseline signal level is high (from Figure 3.4 the hours $h_{\text{start}} \in [10, 23]$).
In general the system is not linear, and if this property is assumed there will be some accuracy loses (as seen on the RMSE of Figures A.1 and A.2).

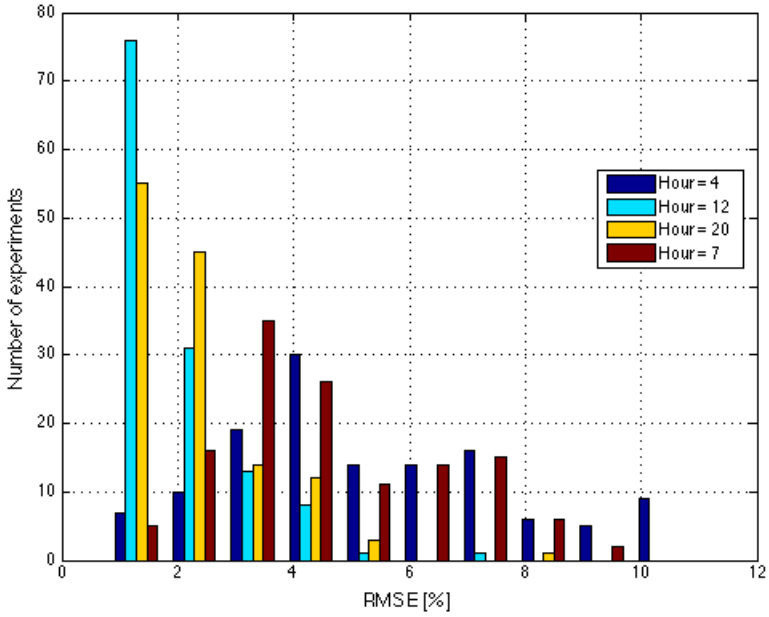

Figure A.1: RMSE histogram for $h_{\text{start}} = \{4, 7, 12, 20\}$

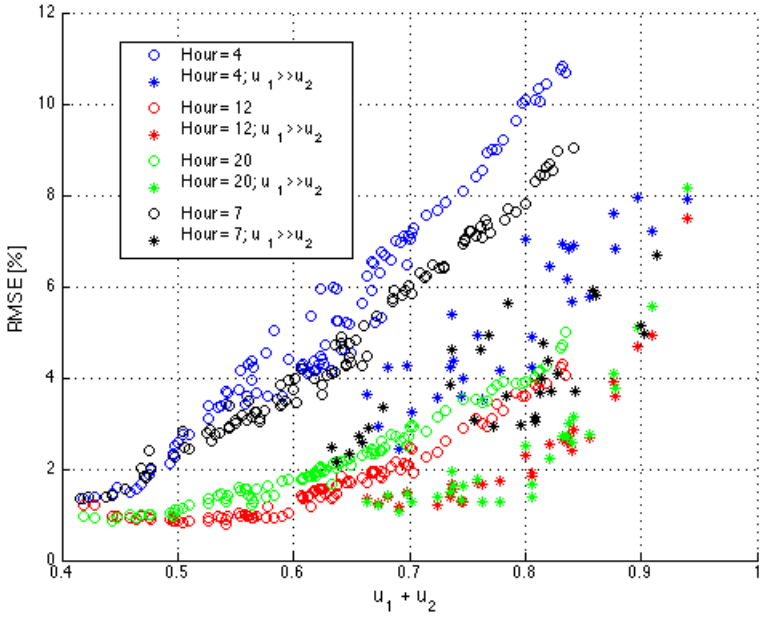

Figure A.2: RMSE for different samples of $\hat{u}_1 + \hat{u}_2$

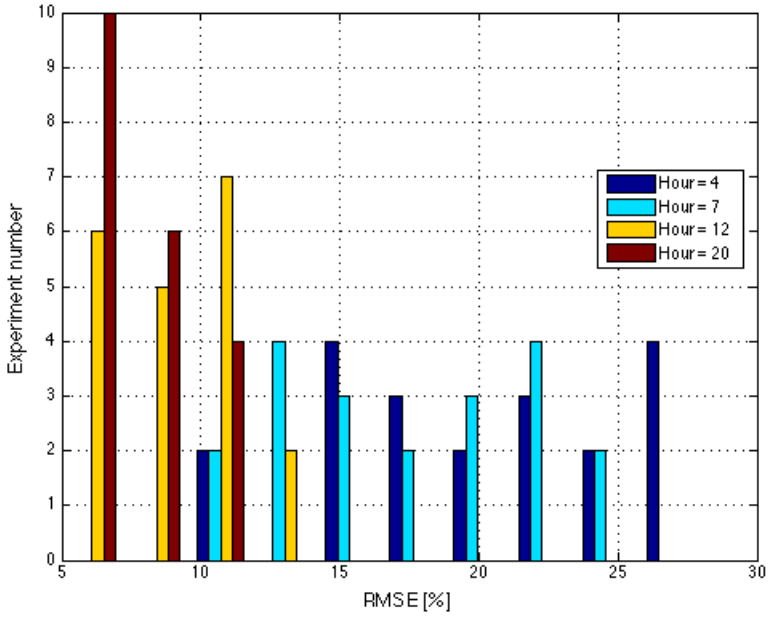

Figure A.3: RMSE histogram for $h_{\text{start}} = \{4, 7, 12, 20\}$